Chapter 2
Compounds of the ReOFeAs Type

2.1 Crystallochemistry and Basic Physical Properties of Doped Compounds

2.1.1 Crystal Structure

The highest values of T_c have been achieved in the row of *Re*OFeAs doped compounds, where *Re* stands for a rare-earth element (Table 2.1). All these compounds possess, at room temperature, a tetragonal structure with the $P4/nmm$ space group. Their crystal structure is formed by repeated FeAs layers, interlaced by the LaO layers. The FeAs layer is, in fact, created by three closely situated atomic planes: the middle one is a quadratic lattice of Fe atoms, sandwiched between two quadratic lattices of As, so that each atom of iron is surrounded by a tetrahedron of arsenic atoms. In other words, the FeAs layer is, in fact, formed by $FeAs_4$ complexes. The FeAs and LaO layers are separated by 1.8 Å.

The crystal structure of LaOFeAs is shown in Fig. 2.1. Lattice parameters for the *Re*OFeAs compounds are given in Table 2.1. As is seen, the tetragonal unit cell is strongly elongated, which explains a strong anisotropy of all its properties and a quasi-bidimensional nature of electronic states. The closest to each Fe atom are those of As, which underway to the next Fe neighbours, so that the electron transfer processes over the Fe sublattice are mediated by the Fe-As hybridization, and the exchange interaction between Fe atoms is of indirect character via the As atoms.

Crystallochemical properties of LaOFeAs compounds are determined by the configuration of the outer electron shells: Fe($4s4p3d$), As($4s4p$), La($6s5d4f$), O($2s2p$). The formal valences of ions are as follows: $La^{3+}O^{2-}Fe^{2+}As^{3-}$.

2.1.2 Electron Doping

On substituting an oxygen atom by fluorine, an extra electron goes into the FeAs layer; such situation is commonly referred to as electron doping. A substitution of lanthanum by, say, strontium, the LaO layer would lack one electron, which can be

Table 2.1 Maximal temperatures of superconducting transitions obtained by doping of the *Re*OFeAs compounds. In the last two lines, the lattice parameters of undoped compounds are given

ReOFeAs	*La*	*Ce*	*Pr*	*Nd*	*Sm*	*Gd*
T_c, K	41	41	52	51.9	55	53.5
Reference	[27]	[9]	[10]	[28]	[11]	[29]
a, *Å*	4.035	3.996	3.925	3.940	3.940	
c, *Å*	8.740	8.648	8.595	8.496	8.496	

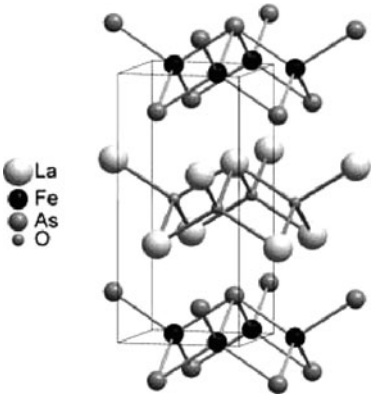

Fig. 2.1 Crystal structure of LaOFeAs

borrowed from the FeAs layer, leaving behind a hole. This would correspond to a hole doping. A re-distribution of electrons between the doped LaO and FeAs layers gives rise to a resulting conductivity of a compound. The nature of carriers can be deduced experimentally from the sign of the Hall constant R_H.

The measurements of the Hall effect have been done on a compound $LaO_{0.9}F_{0.1}$ FeAs [21] with $T_c = 24\,K$ soon after the discovery by Kamihara et al. [8] a superconductivity with $T_c = 26\,K$ on this very compound. In [21], it was concluded that R_H is negative and roughly independent on temperature up to 240 K. This indicates that the conductivity is dominated by electron carriers. From the Hall coefficient measured at $T \approx 100\,K$, the carrier concentration was deduced to be $9.8{\cdot}10^{20}\,cm^{-3}$. The authors of [22] confirmed these estimates. A measurement of R_H on a different sample $LaO_{0.89}F_{0.11}FeAs$ with $T_c = 28.2\,K$, done at a temperature slightly superior to T_c, has shown that the concentration of electron carriers $n \approx 1{\cdot}10^{21}\,cm^{-3}$ [23] does, in fact, coincide with the results of [21, 22] (Fig. 2.2). In the inset of this figure, a temperature behaviour of the Hall coefficient R_H, throughout negative, is shown.

Another example of electron doping is given in Fig. 2.3 [24], where doped and undoped compounds are compared. In both cases, the Hall coefficient is negative. Compounds with other rare-earth elements, e.g. $NdO_{0.82}F_{0.18}FeAs$ [25], well indicate an electron nature of carriers.

A remarkable fact was a discovery of high-T_c superconductivity in the compounds *Re*OFeAs without fluorine doping, but under oxygen deficiency. Thus, [26]

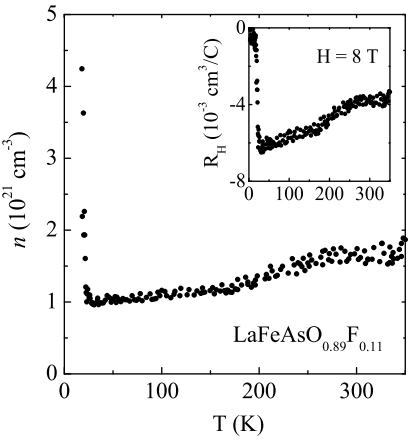

Fig. 2.2 Variation of the number of carriers and the Hall coefficient for the $LaO_{0.89}F_{0.11}FeAs$ compound [23]

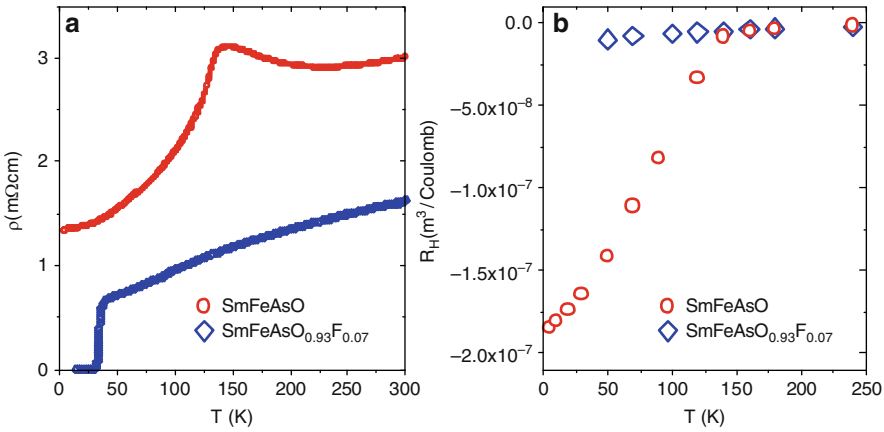

Fig. 2.3 Temperature dependence of resistivity and Hall coefficient for nondoped SmOFeAs and fluorine-doped $SmO_{0.93}F_{0.07}FeAs$ compound [24]

reports a detection of high T_c values in $LaO_{0.6}FeAs$ ($T_c = 28$ K), $LaO_{0.75}FeAs$ ($T_c = 20$ K), and $NdO_{0.6}FeAs$ ($T_c = 53$ K).

In [9–11, 27–29], the data are given concerning the compounds $ReO_{1-\Delta}FeAs$ with Re = Sm,Nd,Pr,Ce,La. Among them, the $SmO_{1-\delta}FeAs$ system indicated the highest $T_c = 55$ K. Hence, the fluorine doping and the oxygen deficiency produce similar effects in the initial stoichiometric compounds: they create electron carriers, suppress antiferromagnetic (AFM) ordering and result in the formation of a superconducting state.

Let us now consider the effect of substitution of a rare-earth element by a heterovalent dopant. A replacement of trivalent Re^{3+} by a quatrovalent substituent results in electron doping. For example, we take a system $Gd_{1-x}Th_xOFeAs$, where Gd^{3+} is substituted by Th^{4+}. At $x \approx 0.1$, a superconductivity with $T_c = 55$ K has

been reported by [30]. Another example of electron doping is $Tb_{1-x}Th_xOFeAs$, where a substitution of Tb^{3+} by Th^{4+} results in $T_c = 52\,K$ [31].

2.1.3 Hole Doping

A completely different situation arises on substituting an Re^{3+} ion by a divalent element. On substitution of La^{3+} in LaOFeAs by Sr^{2+}, we deal with hole doping. The resulting compound, $La_{1-x}Sr_xOFeAs$, at $x = 0.13$ becomes superconducting with $T_c = 25\,K$ [32]. This was the first superconductor in the FeAs-row, obtained by hope doping, as has been confirmed by measuring the Hall coefficient R_H, which turned out in this system to be positive [33].

Apparently, an increase in strontium concentration suppresses the conventional AFM ordering in the pristine compound, and already at $x = 0.03$ the doped state becomes superconducting. T_c grows along with x and at $x \approx 0.11$–0.13 reaches the value of $T_c = 25\,K$. On substituting oxygen by fluorine, $T_c = 26\,K$. We can note a peculiar electron-hole symmetry: on doping a pristine compound by either electrons or holes the T_c grows in roughly similar way. There is, however, a certain difference between two situations. On doping with Sr, a rise of T_c is accompanied by a monotonous increase of the lattice parameters a and c, whereas fluorine doping reduces the lattice parameters [33].

A system $Pr_{1-x}Sr_xOFeAs$ offers another example of the hole doping, on substituting Pr^{3+} by Sr^{2+} [34]. A superconductivity of $T_c = 16.3\,K$ was achieved at the Sr concentration $x \approx 0.20$–0.25. Figure 2.4 shows a temperature dependence of the Hall coefficient, which is, below the room temperature, throughout positive. A similar result occurs in an Nd-based compound on substitution of the latter element with Sr. In an $Nd_{1-x}Sr_xOFeAs$ sample ($0 < x < 0.2$), $T_c = 13.5\,K$ has been achieved at $x \approx 0.2$ [35]. It should be noted that in difference from electron-doped compounds such as $ReO_{1-x}F_xFeAs$ where an increase of x the magnetic ordering is gradually suppressed and superconductivity occurs already at $x < 0.1$, in hole-doped systems

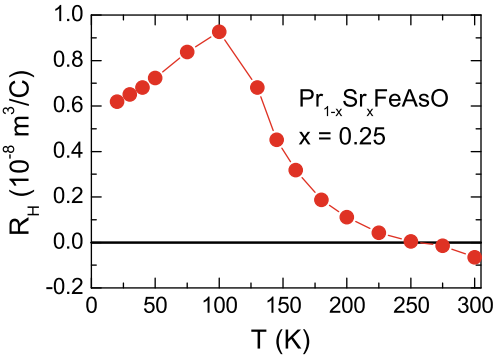

Fig. 2.4 Temperature dependence of the Hall coefficient R_H for the hole-doped $Pr_{0.75}Sr_{0.25}OFeAs$ compound [34]

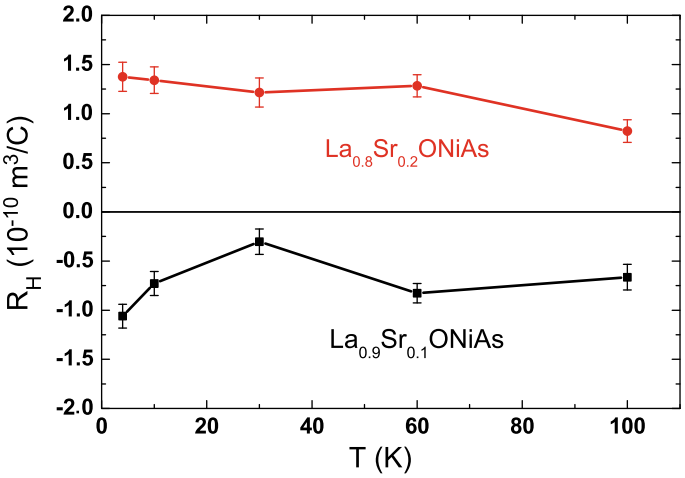

Fig. 2.5 Hall coefficient for two samples of the $La_{1-x}Sr_xONiAs$ compound [36]

an onset of a superconducting state demands higher concentrations of dopant. In this sense, the "electron-hole symmetry" does not hold.

The above discussion of main physical properties in LaOFeAs systems remains valid for those where Ni takes place of Fe, only that the T_c in such systems is much lower. It is noteworthy that the nature of carriers – are they holes or electrons – may vary depending on the dopant concentration (Fig. 2.5).

The LaOFeAs compound can be doped not only by fluorine which substitutes oxygen, but also by elements taking place of lanthanum, e.g. potassium. A doping with potassium adds hole carriers, rather than electrons. In [37], a new method of synthesis of superconducting compounds on the basis of LaOFeAs was suggested, allowing a simultaneous doping with fluorine and potassium. A synthesized compound $La_{0.8}K_{0.2}O_{0.8}F_{0.2}FeAs$ had $T_c = 28.5\,K$.

The examples discussed above show that the superconductivity in FeAs systems might be induced either by electron doping (substituting oxygen by fluorine or due to the presence of oxygen vacancies), or by hole doping (via substituting La by Sr). These tendencies are maintained throughout the whole class of the *Re*OFeAs systems.

2.1.4 Substitutions on the Fe Sublattice

In earlier stages of studying the *Re*FeAsO system, it was shown that the superconductivity is induced by doping on either oxygen or rare-earth sublattice, which both are beyond the FeAs layers. Due to either substitution of oxygen by fluorine, or oxygen deficiency, the FeAs layers are infiltrated by charge carriers, that suppresses antiferromagnetic order of the pristine compound and leads to superconductivity.

In this sense, the new superconductors resemble the cuprates, where substitutions occur outside the CuO_2 planes.

A substitution of Fe atoms in the FeAs layers by Co does as well result in suppression of antiferromagnetism and appearance of superconductivity already at low concentrations of dopant. This feature makes a marked differences of new superconductors from cuprates, in which any intrusion into the CuO_2 planes suppresses superconductivity. In several works appeared simultaneously, astonishing results have been reported on a number of samples of $LaOFe_{1-x}Co_xAs$ [12, 38, 39]. At $x = 0.05$, the antiferromagnetism was suppressed, and at $x \approx 0.1$ a superconductivity with $T_c \approx 10\,\mathrm{K}$ emerged, which further on disappeared at $x > 0.15$. This is confirmed by temperature dependencies of electrical conductivity at different x (Fig. 2.6) [38].

The phase diagram of this system in the (T, x) axes is shown in Fig. 2.7 [39]. It is shown that in the x range corresponding to superconductivity, for $T > T_c$ first a semiconductor-type behaviour is observed, which is followed at $T \approx 100\,\mathrm{K}$ by metallic conductivity. Similar results were obtained for $SmOFe_{1-x}Co_xAs$ [39].

It turns out therefore that Co is an efficient dopant for inducing superconductivity. It is astonishing that superconductivity persists at quite high degree of disorder (broad interval of x) that apparently is an argument in favour of a non-standard symmetry of the order parameter, which is not sensitive to magnetic impurities [40]. It is interesting to note that for $x = 1$ the system becomes ferromagnetic with $T_c \approx 56\,\mathrm{K}$ [38].

Note that electronic structure calculations for $LaOFe_{1-x}Co_xAs$ have appeared [41], which show that the Co doping displaces the Fermi level from its position at the slope of the partial density of Fe3d states into a more flat region. This circumstance explains a suppression of the SDW transition in the initial LaOFeAs on doping of its Fe sublattice.

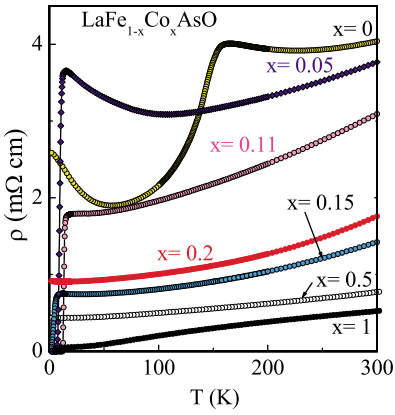

Fig. 2.6 Temperature dependence of electrical resistivity of the $LaOFe_{1-x}Co_xAs$ compound at different cobalt concentrations [38]

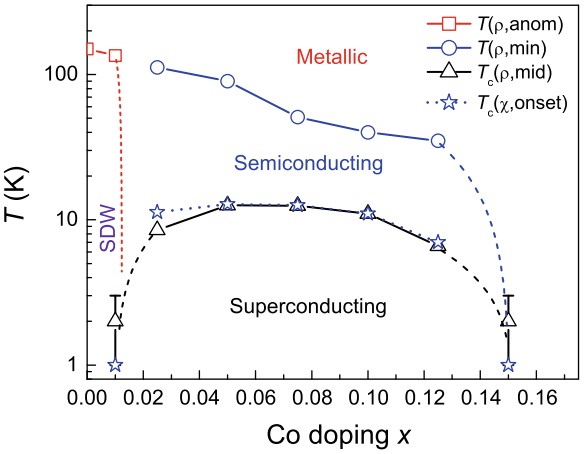

Fig. 2.7 Phase diagram of $LaOFe_{1-x}Co_xAs$ in the (T, x) plane [39]

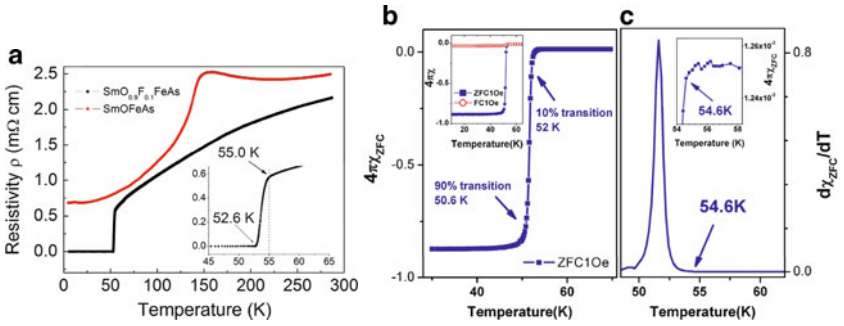

Fig. 2.8 Manifestation of superconducting state in the $SmO_{0.9}F_{0.1}FeAs$ compound as revealed by temperature dependence of (**a**) electrical resistivity, (**b**) magnetic susceptibility χ, (**c**) the derivative of χ in temperature [11]

2.1.5 Superconducting Transition Temperature

Now we turn to a more detailed description of superconducting properties in FeAs systems. How does a superconducting state in a doped material reveal itself in experiment? Let us take as an example the $SmO_{1-x}F_xFeAs$ compound in which at $x = 0.1$ the highest so far value of $T_c = 55$ K has been obtained [11]. Figure 2.8 shows the results of three different measurements: a sharp drop of electrical conductivity on lowering the temperature, a sharp appearance of diamagnetic response χ in applied magnetic field, and a sharp peak in the $d\chi/dT$ derivative. All three anomalies occur near the same temperature, which is, accordingly, the superconducting transition temperature. The curves as in Fig. 2.8 are typical for all superconducting systems on the FeAs basis. For comparison, corresponding curves for a group of

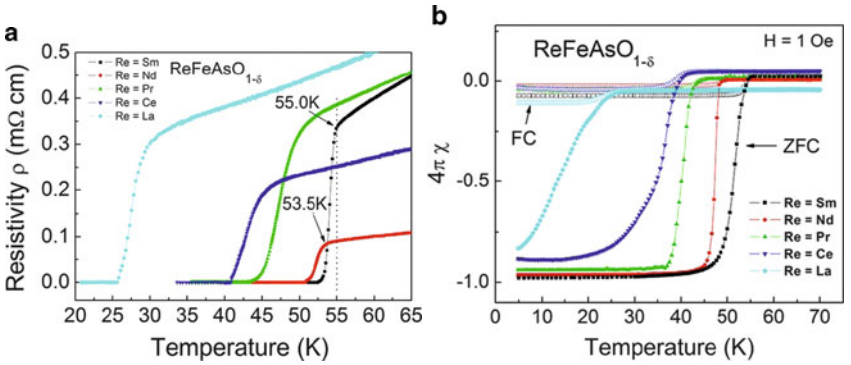

Fig. 2.9 Electrical resistivity (**a**) and magnetic susceptibility (**b**) of superconducting $ReO_{1-x}FeAs$ compounds with oxygen deficiency, as function of temperature [42]

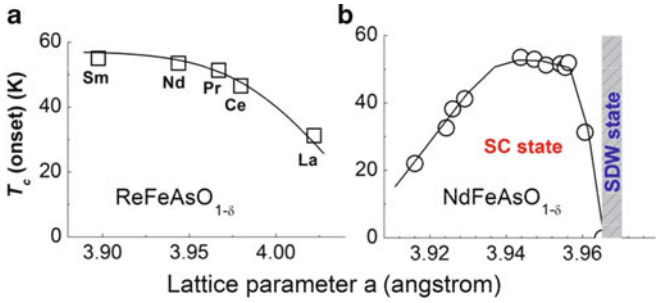

Fig. 2.10 T_c in the row of $ReO_{1-\delta}FeAs$ compounds as function of the lattice parameter a [42]

*Re*OFeAs compounds with different rare-earth constituents are shown in Fig. 2.9 [42]. The behaviour of electrical conductivity and magnetic susceptibility in the vicinity of T_c is similar between different systems. We note that, differently from the SmOFeAs system of Fig. 2.8 which was doped with fluorine, all superconducting compounds collected in Fig. 2.9 are deficient in oxygen. Despite different nature of dopants – fluorine substitution or oxygen vacancies – the manifestation of superconducting state in the temperature dependence of electrical conductivity and magnetic susceptibility is identical for both systems. It is instructive to compare the superconducting transition temperatures throughout a row of compounds with different rare-earth elements and hence lattice parameter a (Fig. 2.10). We see that T_c decreases with the rise of a (due to the increase of the element's ionic radius). For a given rare-earth constituent, T_c depends on the number of oxygen vacancies δ. In a synthesized compound, the vacancy concentration is revealed by the lattice parameter a (Fig. 2.10b).

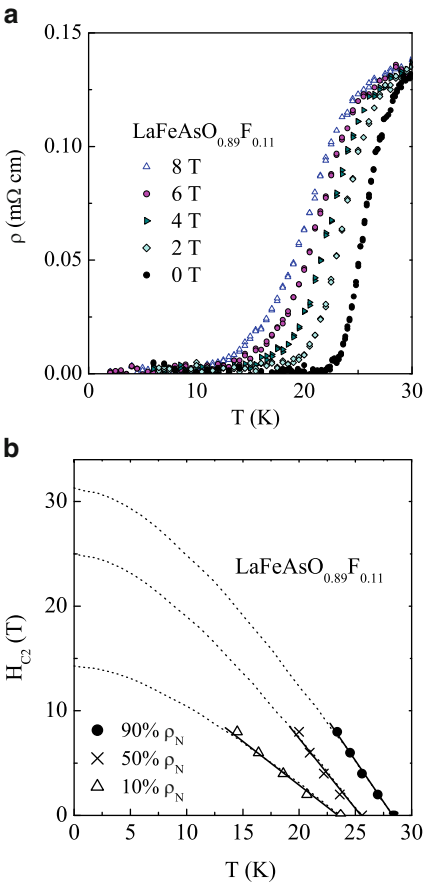

Fig. 2.11 Temperature dependence of (**a**) electrical resistivity in different magnetic fields, and (**b**) the values of H_{c2} extracted from these data, for $LaO_{0.89}F_{0.11}FeAs$ [23]

2.1.6 Critical Fields

Besides high transition temperatures, the FeAs-type compounds possess very high critical fields values. Consider, as an example, a study of the upper critical field H_{c2} in polycrystalline sample of $LaO_{0.98}F_{0.11}FeAs$ with $T_c = 28.2$ K [23].

H_{c2} is estimated from the data on the temperature dependence of electrical resistivity in magnetic field. In Fig. 2.11a, such data in the field range up to 8 T are given, and in Fig. 2.11b, the $H_{c2}(T)$ results extracted from the latter. It is seen from Fig. 2.11a that the interval of the drop in resistivity shifts towards lower temperatures on applying the field, that is typical for II order superconductors. The superconducting transition temperature $T_c(H)$ is defined by the condition that $\rho(T_c, H)$ equals a certain fraction (percentage) of resistivity ρ_N in the normal phase, for a given field magnitude H. The thus defined values of $T_c(H)$ for $\rho = 10$, 30 and 90% of ρ_N are shown in Fig. 2.11b along with the critical fields $H_{c2}(T)$. In all cases, $H_{c2}(T)$ exhibit linear dependence without any tendency towards saturation.

The slope $dH_{c2}/dT\ |_{T=T_c}$ equals -0.87 T/K for $\rho = 10\%\rho_N$, -1.41 T/K for $\rho = 50\%\rho_N$ and -1.59 T/K for $\rho = 90\%\rho_N$. In the BCS theory, the H_{c2} is linear in T in the vicinity of T_c and saturates towards $T = 0$. According to the Werthamer–Helfand–Hohenberg formula [43],

$$H_{c2}(0) \approx -0.693\, T_c \left.\frac{dH_{c2}}{dT}\right|_{T=T_c}. \tag{2.1}$$

The dashed lines in Fig. 2.11b are extrapolations of linear experimental curves towards the thus calculated values of $H_{c2}(0)$. For $\rho = 90\%\rho_N$, the $H_{c2}(0)$ exceeds 30 T. From the known Ginsburg–Landau formula for the correlation length $\xi(0) \approx (\Phi_0/2\pi H_{c2})^{1/2}$, where Φ_0 is a flux quantum, an estimation follows: $\xi(0) \approx 48$ Å for H_{c2} $(10\%\,\rho_N)$, $\xi(0) \approx 36$ Å for H_{c2} $(50\%\,\rho_N)$, $\xi(0) \approx 33$ Å for H_{c2} $(90\%\,\rho_N)$. These values are comparable to those measured in cuprates for corresponding values of T_c.

Measurements of the Hall constant on the same sample revealed its negative sign (that corresponds to electron carriers) and carriers concentration of $\approx 1.7{\cdot}10^{21}$ cm^{-3} at room temperature and $\approx 1{\cdot}10^{21}$ cm^{-3} at a temperature just above T_c (assuming a single carriers band).

The above data concerning the sample studied of $LaO_{0.89}F_{0.11}FeAs$ are quite representative for the whole series of superconducting compounds $ReO_{1-x}F_xFeAs$. Thus for $NdO_{0.82}F_{0.18}FeAs$ with $T_c = 51$ K [44], $H_{c2}(48\,\text{K}) = 13$ T has been measured, and the critical field $H_{c2}(0)$ estimated after (2.1) turned out to be within 80–230 T. Measurements on a single crystal of the same composition [45] revealed a large anisotropy of H_{c2}.

The critical fields estimated after (2.1) for the field directions in the basal plane (ab) and along the tetragonal axis (c) are: $H_{c2}^{ab}(0) \approx 304$ T and $H_{c2}^{c}(0) \approx 62$–70 T. The measurements on a Sm-based compound confirmed high values of H_{c2}. Thus for a sample $SmO_{0.85}F_{0.15}FeAs$ with $T_c = 46$ K, the measurements of specific heat in the fields of up to 20 T gave [46] $[dH_{c2}/dT]_{T=T_c} = -5$ T/K, that according to (2.1) gives an estimate $H_{c2}(0) = 150$ T. For another sample, $SmO_{0.7}F_{0.3}FeAs$ [47] with $T_c = 54.6$ K, the estimated $H_{c2}(0)$ is even higher: $H_{c2} \approx 200$ T. A detailed review of (H, T) phase diagrams of FeAs compounds can be found in [48].

2.1.7 *Effect of Pressure on the T_c*

Soon after the discovery of superconductivity in $LaO_{1-x}F_xFeAs$ it was reported that in the compound with $x = 0.11$, the T_c increases under applied pressure and reaches the maximum value of 43 K at 4 GPa [49]. It was suggested that the lattice compression is responsible for this effect. Indeed, in *Re*OFeAs compounds the atoms of rare-earth element have smaller radius than La, and T_c in these compounds is markedly higher, exceeding 50 K. In a subsequent work [50], the measurements of electrical conductivity in LaOFeAs under high pressures, up to 29 GPa, have

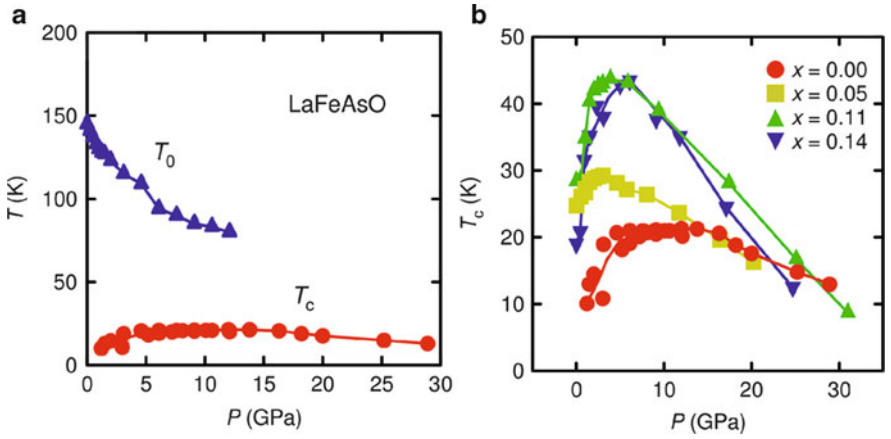

Fig. 2.12 (**a**) (T, P) phase diagram for LaOFeAs, obtained from the measurements of electrical resistivity at different pressures [50]; (**b**) variation of T_c with pressure in $LaO_{1-x}F_xFeAs$ compounds. The data for doped compounds are taken from [49, 51]

been done. The results concerning the variation of the temperatures of structural (magnetic) phase transition T_0 and of the superconducting transition temperature, extracted from the raw data on $\rho(T)$ at different pressures, are shown in Fig. 2.12.

The (P, T) phase diagram shown in Fig. 2.12a resembles the (x, T) phase diagram for doped $LaO_{1-x}F_xFeAs$ compounds [8]. This similarity may be explained by an observation that the oxygen substitution with fluorine, beyond modifying the carriers density, results in reducing the lattice constant. Thus, as $x = 0.05$ the unit cell squeezes from $0.14186\,nm^3$ that is accompanied by an appearance of superconductivity with $T_c = 24\,K$ [8]. According to the variation of the unit cell volume under pressure [51], the above variation corresponds to a pressure of $\sim$0.3 GPa. Correspondingly, in the context of merely changing the volume, the substitution of oxygen with fluorine is more efficient in suppressing structural and magnetic phase transitions and the onset of superconductivity that an effect of external pressure.

As is seen from Fig. 2.12b, the maximal $T_c = 21\,K$ in stoichiometric compound LaOFeAs is achieved at the pressure of $\sim$12 GPa. As regards the variation of T_c with pressure in doped compounds, it first rises with pressure, passes through maximum and falls down. A similar behaviour of T_c under pressure is observed in $LaO_{1-x}F_xFeAs$ of a different composition, as well as in oxygen-deficient LaOFeAs compounds (Fig. 2.13). The latter have maximal $T_c \sim 50\,K$ at the pressure of 1.5 GPa [52].

A relation between the changes of T_c under pressure and variation of the lattice parameter is shown in Fig. 2.14. At high pressures ($P > 10$ GPa), the lattice parameters and T_c in the compound investigated $LaO_{0.9}F_{0.1}FeAs$ do decrease linearly [53].

A similar behaviour of T_c under pressure was observed in another compound type, LaOFeP. At the ambient pressure, T_c in doped $LaO_{1-x}F_xFeP$ compounds is

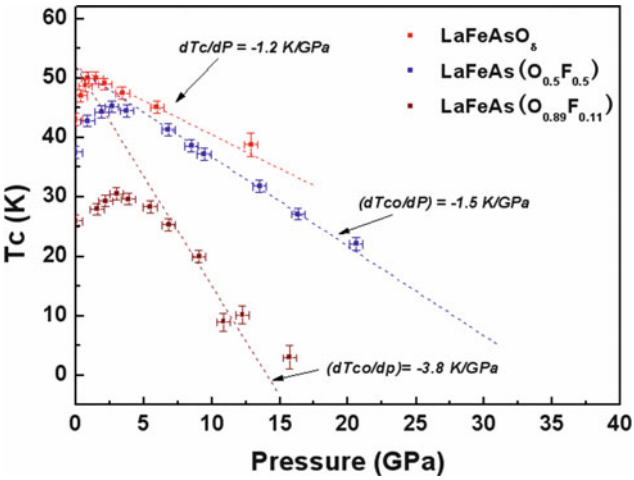

Fig. 2.13 Variation of the superconducting transition temperature with pressure for two $LaO_{1-x}F_xFeAs$ compounds and a $LaO_\delta FeAs$ compound with oxygen vacancies [52]

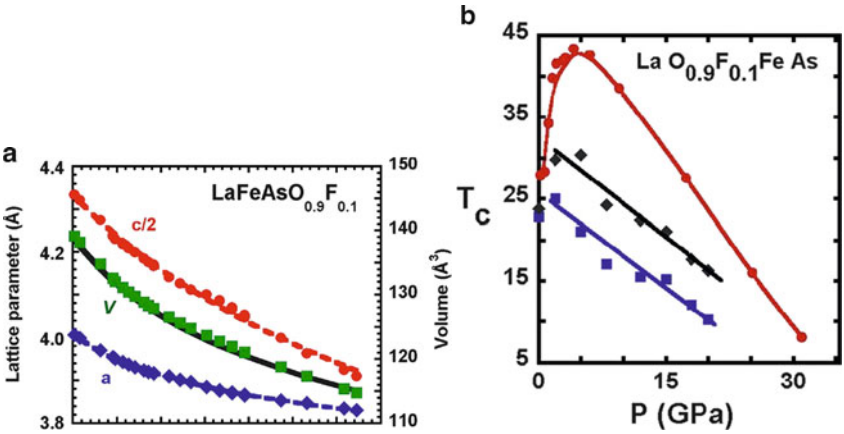

Fig. 2.14 Variation under pressure of (**a**) lattice parameters, and (**b**) superconducting transition temperature, for the $LaO_{0.9}F_{0.1}FeAs$ compound [53]

2–7 K. On applying the pressure, T_c rises rapidly, achieving 8.8 K already at $P = 0.8$ GPa, after which it falls down at the rate $dT_c/dP > 4$ K/GPa [54].

Finally, we discuss an aspect of chemical pressure which occurs on a substitution of an ion in the compound by another ion of a smaller radius. In this case, the shrinking of the lattice parameter is observed as the dopant concentration grows. This situation is illustrated by Fig. 2.15, taken from [55].

Yttrium has smaller ionic radius than lanthanum, therefore replacing the latter by the former reduces the lattice parameter a. As is seen from the figure, T_c grows with the yttrium concentration, whereas T_N decreases. This trend is common for all

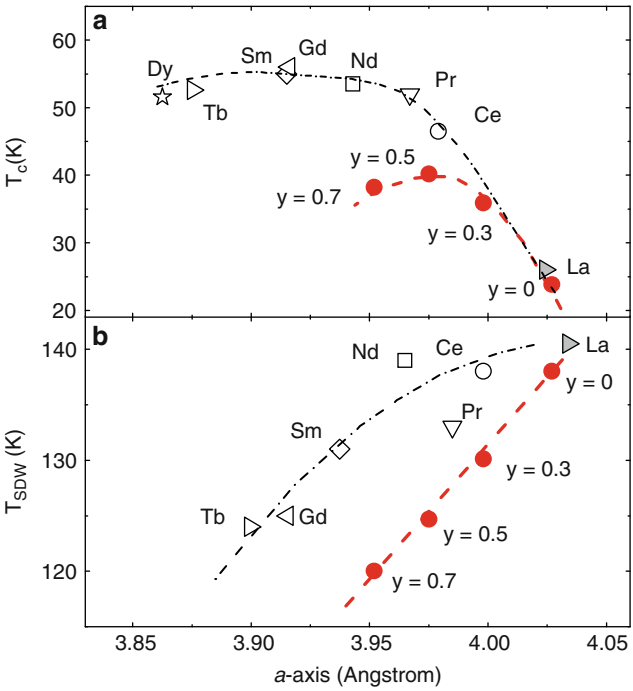

Fig. 2.15 (**a**) T_c and (**b**) T_N for *Re*OFeAs compounds as functions of the lattice parameter. *Black dots* indicate the values of T_c and T_N for the $La_{1-y}Y_yF_{0.15}FeAs$ compound at the levels of yttrium concentration $y = 0$; 0.3; 0.5; 0.7 [55]

$ReO_{1-x}F_xFeAs$ compounds, which exhibit a maximum T_c value at some optimal fluorine doping x.

A doping of the stoichiometric compound LaOFeAs with yttrium up to $y \leq 0.7$ does not lead to superconductivity, because an effect of chemical pressure is by far weaker than that of the fluorine doping. On yttrium doping of already superconducting compound $LaO_{1-x}F_xFeAs$, T_c increases from 24 to 40 K. Obviously, this happens not so much due to a decrease of the lattice parameter (chemical pressure) as because of adding new carriers to the compound, as La is partially replaced by Y. Therefore, the role of chemical pressure at the onset of superconductivity in FeAs-based compounds is considerably limited, in comparison with the effect of doping by heterovalent elements.

A particularly interesting behaviour of superconductivity under pressure is observed in Ce-containing compounds. In general, compounds with Ce do often exhibit anomalies induced by the Kondo screening of localized moments of the $4f$ shell of Ce atoms. In metallic Ce, an isostructural $\alpha \rightarrow \Gamma$ phase transition under pressure occurs, whose nature is purely electronic one, induced by a change of the Ce valence [56].

In [57], based on a thorough study of transport properties and X-ray absorption spectra under pressure, a competition of superconductivity and Kondo screening was found in the $CeO_{0.7}F_{0.3}FeAs$ compound. On increase of pressure, the superconducting transition temperature is gradually decreasing, and from $P = 8.6\,\text{GPa}$ on it drops abruptly, reaching zero at $P = 10\,\text{GPa}$. XAS studies show a re-distribution of statistical weight from the main absorption line towards the satellite, indicating an appearance of the $4f^0$ states in the main bulk of the $4f^1$ states of Ce ions. A similar behaviour is observed in metallic Ce at the $\alpha \rightarrow \Gamma$ transition, see [56].

Therefore, the X-ray absorption spectra reveal the Kondo screening of the localized moments at Ce ions, caused by pressure. The spectra of the superconducting state are similar to the XAS of pure Ce. Guided by this analogy, the authors of [57] arrived at a conclusion that the reason of the suppression of T_c by pressure in $CeO_{0.7}F_{0.3}FeAs$ is in an emergence of a state with Kondo singlets, that expels the state with the Cooper pairs. Therefore, a quantum phase transition under pressure takes place, driven by a screening of localized moments of the Ce$4f$ shell by the Fe$3d$ electrons.

We mention in this relation the work [58], in which, in non-superconducting $CeOFeAs_{1-x}P_x$, two quantum critical points have been found, under the variation of the phosphorus content x. In the (T, x) phase diagram, for $x < 0.37$ an antiferromagnetic phase was detected with an ordering of localized moments at Fe and Ce sites. Further on, in the $0.92 < x < 1.00$ range a non-magnetic state with heavy fermions come about, induced by the Coulomb screening.

2.2 Magnetic Properties

2.2.1 Magnetic Structure

Stoichiometric *Re*OFeAs compounds are antiferromagnetics. The first indications of a possibility of magnetic ordering in LaOFeAs stem from measurements of temperature dependences of electrical conductivity and magnetic susceptibility, which exhibited anomalies near $T \approx 150\,\text{K}$. At this temperature, a structure transition from tetragonal into orthorhombic phase have been detected. It was initially suggested that the magnetic ordering occurs at the same temperature. By now, full neutron diffraction studies done at a nuclear reactor in Oak Ridge clarified the situation [59]. At $T \approx 155\,\text{K}$, indeed, a structural transition occurs with changing the symmetry from tetragonal space group $P4/nmm$ to monoclinic $P112/n$ at lower temperatures (in some cases a transition into orthorhombic phase *Cmma*) has been detected).

It turned out that magnetic phase transition happens at a lower temperature, $T_N = 137\,\text{K}$. In neutron diffraction patterns, magnetic reflects (103), corresponding to doubling the primitive cell along the c axis, have been found. The main result of the study of LaOFeAs is shown in Fig. 2.16, where points and squares mark the

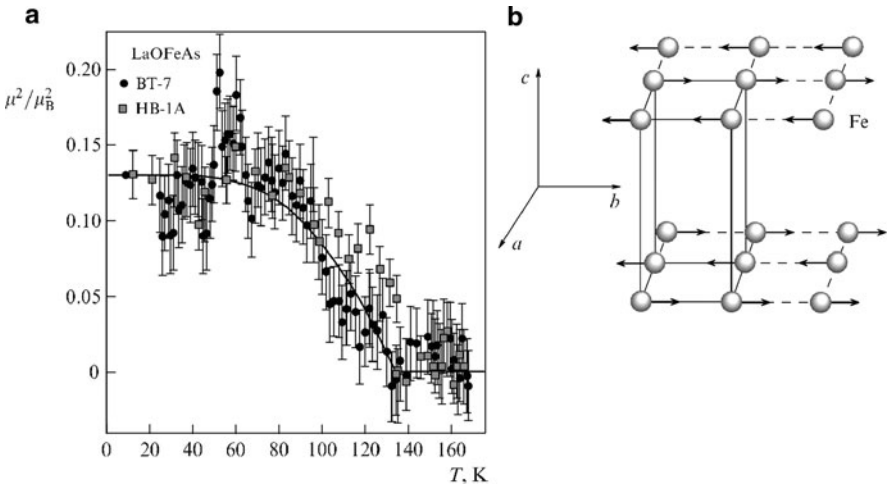

Fig. 2.16 (**a**) Intensity of the magnetic Bragg peak in LaOFeAs according to neutron diffraction data, depending on temperature [59]. Experimental *dots* and *squares* correspond to measurements at different diffractometers. (**b**) Magnetic ordering in the Fe sublattice

temperature dependence of the magnetic reflex, which scales as the square of the magnetic order parameter. The inset at the top shows the magnetic structure formed in the Fe sublattice.

As is shown from the Fig. 2.16, the resulting magnetic structure is an antiferromagnetic alteration of ferromagnetic chains (stripes) in the basal plane. This structure quite agrees with theory predictions following from band structure calculation of this compound [60], even as the compound is in fact metallic. In this sense, the magnetic ordering in FeAs compounds is drastically different from that in cuprates. Cuprate compounds at the stoichiometry exhibit rather conventional antiferromagnetic ordering in basal planes, whereby magnetic moments of Cu atoms are set antiparallel to the moments of their nearest neighbours in the copper sublattice. Stoichiometric cuprates are Mott insulators.

As was earlier pointed out, a doping of cuprates destroys long-range magnetic ordering and results at the onset of superconducting state. The situation is similar in the FeAs systems. Neutron diffraction studies of doped superconducting compound $LaO_{1-x}F_xFeAs$ ($T_c = 26$ K) showed an absence of magnetic order. Therefore, similarly to how it is in cuprates, the superconductivity occurs in the vicinity of magnetic phase transition that indicates an important role of antiferromagnetic fluctuations in electron pairing. Magnetic ordering as shown in Fig. 2.16 has been also found in another stoichiometric compound, namely in NdOFeAs with $T_N = 141$ K [61].

In both these compounds (with $Re =$ La, Nd), the magnetic moment per Fe atom, at low temperatures, is anomalously small: $0.36\,\mu_B$ for the La-based and $0.25\,\mu_B$ for the Nd-based compound, whereas according to theory predictions it is expected to be $\sim 2\,\mu_B$ [62, 63]. This discrepancy marks a thus far persisting problem. Even as it is evident that an occurrence of frustrations (two antiferromagnetic interactions

between Fe atoms in the basal plane) might reduce the mean magnetic moment somehow, a reduction by a factor of five is difficult to understand. We note, however, an existence of calculations of electron density done within the LDA+U scheme with negative U value (to be understood as $U_{eff} = U - J$), which result in a substantial reduction of the magnetic moment [12].

Neutron diffraction studies of $CeO_{1-x}F_xFeAs$ [9] did in part confirm an antiferromagnetic structure of other compounds. More precisely, the spins of Fe atoms in the basal plane do build ferromagnetic stripes, alternating antiferromagnetically as shown in Fig. 2.16, and this magnetic structure is repeated or alternate along the c axis. Presumably, it is related to a special role of Ce atoms in compounds, because of the tendency of valence electrons of cerium to easily hybridize with other electrons. It is noteworthy that the Fe magnetic moments in this compound are higher, of about 1 μ_B. A study of a fluorine-doped compound revealed phase diagram rather similar to that of cuprates.

Besides the above cited publication, one should mention the studies of magnetic ordering in the SmOFeAs by magnetic measurements [64]. The stoichiometric compound SmOFeAs shows an anomaly in magnetic susceptibility as $T \approx 140\,\mathrm{K}$ due to an onset of antiferromagnetic order. At $T \approx 6\,\mathrm{K}$, another peak in $\chi(T)$ is detected, which reveals an antiferromagnetic ordering established in the Sm sublattice. In the doped compound $SmO_{0.85}F_{0.15}FeAs$ the antiferromagnetic ordering in the FeAs planes is suppressed, whereas the ordering in the Sm sublattice persists even as the material becomes a superconductor with $T_c = 52\,\mathrm{K}$. Therefore, we face a situation when superconductivity and magnetic ordering so coexist, even if they manifest themselves on different electron subsystems, belonging to Fe and Sm atoms, respectively. It is interesting to note that the magnetic susceptibility of the SmOFeAs system has a Curie–Weiss contribution from Fe atoms, from which the magnitude of magnetic moments at the latter can be estimated to be about 1.4 μ_B.

2.2.2 *Theoretical Explanation of Long-Range Magnetic Ordering in ReOFeAs*

Shortly after clarifying the magnetic structure of the LaOFeAs compound in a neutron diffraction experiment [59], its theoretical explanation was given by Yildirim [65]. This explanation is based on the LDA total energy calculations for possible frustrated magnetically ordered phases of the compound in question, along with an idea that frustrations can be removed by crystal lattice distortions.

An initial suggestion was that the J_1 exchange interaction between the nearest Fe atoms on the square lattice of undoped LaOFeAs and the J_2 interaction between next-nearest neighbours, is antiferromagnetic. This immediately puts forward two schemes of antiferromagnetic ordering, AFM1 and AFM2, shown in Fig. 2.17. An analysis of the exchange energies expressed consistently with the localized Heisenberg model of classical spins does easily result in a conclusion that the AFM1 is stable for $J_1 \gg J_2$ and AFM2, on the contrary, for $J_2 \gg J_1$. This result

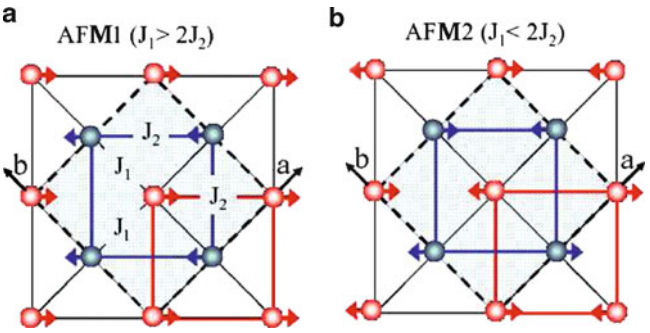

Fig. 2.17 Two possible types of antiferromagnetic ordering under antiferromagnetic exchange interactions J_1, J_2 [65]

is understandable, because in case of large J_1 the highest priority is to satisfy the antiferromagnetic ordering between nearest neighbours, leaving the weaker J_2 interaction frustrated. In the opposite case of large J_2, the AFM2 structure assures antiferromagnetic spin setting between the next-nearest neighbouring Fe atoms, at the expense of leaving the J_1 interactions frustrated.

In both cases, the antiferromagnetic structure of the whole plane can be considered as two interlaced antiferromagnetic sublattices. A further difference between the two structures is the following. In the AFM2 structure, each Fe atom is surrounded by other Fe nearest neighbours, so that its spin finds itself in zero exchange field, hence the mutual orientation of spins in two sublattices is not fixed, and we deal with fully frustrated situation. It is known that in frustrated magnetic systems, a frustration in nearly all cases is lifted either by structure distortions, or by thermic or quantum fluctuations [66, 67]. Therefore if the AFM2 ordering gets materialized, one could expect ordered structure distortions of the tetragonal lattice that was indeed detected experimentally [59]. Such simple yet fruitful considerations was put forward on the basis of the localized model, despite the fact that the latter cannot be, strictly speaking, attributed to the LaOFeAs compound, which is not an insulator but a metal. Therefore, it was essential to probe energies of emerging magnetic structures by calculations done within the itinerant model as well. In [65], total energies of four different phases have been calculated: the nonmagnetic (NM) and ferromagnetic (FM) ones, along with the antiferromagnetic AFM1 and AFM2. The calculations have been done in the LDA. The energies calculated for these four phases in dependence on the fixed mean moment, m, of the spin projection $\langle S^z \rangle$ at the Fe atom onto the quantization axis have shown that the AFM2 structure has indeed the lowest energy, which is achieved at $m = 1$. The calculations in which the mean spin was not fixed revealed the minimum at somehow smaller value of $m = 0.87\,\mu_B$. We note in passing that this value does still exceed the experimental value of $0.36\,\mu_B$ by a factor of nearly two.

A comparison of calculated total energy values with the formulas following from the localized model with two exchange interactions, J_1 and J_2, permits to extract the

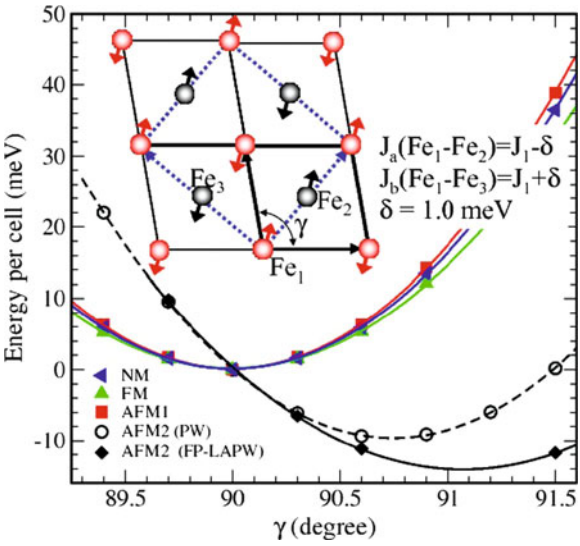

Fig. 2.18 Total energy per elementary unit depending on the angle γ for four phases: NM, FM, AFM1, and AFM2. In the inset, a distorted magnetic structure with the AFM2 magnetic ordering is shown [65]

values of the latter. Both interactions turned out to be antiferromagnetic and of the same order of magnitude, whereas however $J_2 > 1/2\,J_1$, confirming the preference towards the AFM2 type of ordering.

Let us now discuss the effect of lattice distortions onto the magnetic structure. Orthorhombic distortions of the tetragonal lattice, like those found in LaOFeAs simultaneously with the onset of a magnetic ordering, can be realized by varying the angle Γ (Fig. 2.18) in either sense away from 90° [65]. In this case, the distance between Fe_1 and Fe_2 atoms increases, and between Fe_1 and Fe_3 decreases. The exchange integral J_1 gets smaller between atoms situated along the a direction and larger along the b direction. This can be casted into the formula $J_a = J_1 - \delta$, $J_b = J_1 + \delta$, whereby the net exchange energy of crystal is decreasing, exploiting the changes in exchange interaction between spins along the a direction and along the b direction. The energies of all four phases, calculated in the LDA depending on the angle Γ, are shown in Fig. 2.18. It is shown that the AFM2 ordering has the lowest energy for $\Gamma = 91°$. The experimental value is 90.3°, whereby the calculated value of the mean spin $m = 0.48\,\mu_B$ is reasonably close to the experimental one, $0.36\,\mu_B$. The structure distortion reduces the magnitude of the local moment in the AFM2 ordering from 0.87 to $0.48\,\mu_B$. The density of states at the Fermi level in distorted phase gets almost doubled. Therefore, a competition of two antiferromagnetic interactions J_1 and J_2 in pristine LaOFeAs compound is resolved by an orthorhombic lattice deformation, which stabilizes the AFM2 magnetic structure. This picture yields the lattice distortion parameters and mean magnetic moment values, which are close to the experimental data.

A problem of anomalously small values of mean magnetic moments on Fe atoms was discussed in [68, 69]. In [68], the methods of Mössbauer spectroscopy and muon spin rotation (μSR) were applied to minutiously measure the temperature

dependence of the sublattice magnetization in undoped LaOFeAs and the SDW order parameter. From these two measurements, a mean magnetic moment per Fe site has been extracted to be $0.25\,\mu_B$. Calculations which used the four-band model of an antiferromagnet in the mean-field approximation resulted in a higher value, $0.33\,\mu_B$, – a qualitatively expected trend, due to the fact that the mean-field theory neglects the fluctuations. In [69], calculations of the electronic structure of LaOFeAs and of the magnetic moments on Fe atoms were done under assumption of different AFM structures, within both LDA and GGA. Specifically, three structures have been inspected, AFM-1, AFM-2 and AFM-3, different in the orientation of magnetic moments of adjacent Fe atoms within the basal plane and between neighbouring planes. One of the structures, AFM-3 with the magnetic cell doubled along the c axis, was that deduced from the neutron diffraction studies. The calculations of electronic structure and mean moments on Fe atoms for each of the three AFM structures have been done for different volumes of the primitive cell, i.e. for different ambient pressures.

The results were unexpected. At fixed cell volume, the mean magnetic moments turned out to be very sensitive to the type of AFM structure. In the vicinity of the equilibrium volume, the magnetic moment decreased strongly, especially in the AFM-1 structure. For the really existing AFM-3 structure, the magnitude of the mean magnetic moment changed by a factor of three within the pressures range of ± 5 GPa. At the pressure of 5 GPa, the calculated moments agree with the experimentally measured ones. Through the pressure range of -10 to $+10$ GPa, the Fe magnetic moment falls down from the maximal possible one ($2\,\mu_B$) to nearly zero. Therefore, an increase of negative pressure (i.e. lattice dilatation) is expected to induce a large rise of the magnetic moment. This effect could have been checked on hydrogenated samples, where the hydrogen absorption permits to imitate a negative pressure.

It is remarkable that the electronic structure does not substantially change within broad range of pressures, whereas the magnetic moment varies considerably. This indicates that the magnetic state of the compound (its magnetic structure and the magnitude of mean magnetic moment) results from a delicate equilibrium between the kinetic energy, which determines the electronic structure within the LDA, and inter-electron interaction. Therefore, a description of FeAs-type compounds within a purely localized spins model, like the Heisenberg one, might be quite problematic: these compounds are with certainty rather itinerant magnets.

The main problem concerning the nature of magnetic properties of the FeAs-compounds is explaining the smallness of the mean magnetic moment at Fe atoms in the magnetically ordered SDW state, and finding out the structure of magnetic excitations spectrum in the doped compounds.

In relation with the question of magnetic moments, we draw attention to [70] in which, within the self-consistent spin waves theory, an attempt has been done to calculate the mean moment $\langle S^z \rangle$ at the Fe atoms, proceeding from the fully localized Heisenberg model. Hereby, four different exchange interactions have been considered. Two of them are between nearest neighbours, J_{1a} along the chain of identically magnetized atoms and J_{1b} – between those nearest neighbours, which belong to the

chains of opposite spin direction. Further on, J_2 is between next-nearest neighbours in the ab plane, and J_c between the nearest neighbours along the c direction.

In [70], via the Green's function of spin waves, self-consistent equations for $\langle S^z \rangle$ have been obtained. From these equations, in the limit $\langle S^z \rangle = 0$, a formula for the Neél temperature T_N in terms of the four exchange interaction parameters is derived. The authors of [70] proceeded from the experimental value $T_N = 138\,\mathrm{K}$ for the LaOFeAs compound and, making use of the self-consistent equation for $\langle S^z \rangle$, estimated the most probable magnitudes of exchange interactions: $J_{1b} = 50 \pm 10\,\mathrm{meV}$, $J_{1a} = 49 \pm 10\,\mathrm{meV}$, $J_2 = 26 \pm 10\,\mathrm{meV}$, $J_c = 0.020 \pm 0.01\,\mathrm{meV}$. A solution of the equation for $\langle S^z \rangle$ for these parameter values yielded the temperature dependence of $\langle S^z \rangle$ throughout the whole temperature interval, up to T_N. For $T = 0$, it turned out that $\langle S^z \rangle = 0.7$. In this calculation, the value of atomic spin $S = 1$ at the Fe atom has been taken, which most closely corresponds to the value of the magnetic moment calculated from first principles.

Therefore, the spin fluctuations do decrease, for chosen values of exchange parameters, the magnitude of $\langle S^z \rangle$ as in the SDW ground state from $\langle S^z \rangle = 1$ to $\langle S^z \rangle = 0.7$. This spin contraction is much weaker than that in fact observed in LaOFeAs and other compounds of this type. An additional reduction of the mean moment at Fe atoms is, most probably, a consequence of a more itinerant character of magnetism in these systems.

In what concerns the magnetism of rare-earth ions in *Re*OFeAs systems, a question remains open: why, throughout the series of superconducting $ReO_{1-x}F_xFeAs$ compounds with localized moments (Re = Ce, Pr, Nd, Sm), the T_c values stay higher than in the La-based compound? Systematic studies of rare-earth magnetism in these systems were performed in [71] using μSR experiments and a symmetry analysis. Different combinations of magnetic orderings in rare-earth and Fe sublattices have been taken into consideration. A strong influence of the magnetic ordering in the *Re*-sublattice onto the magnetism of the Fe-sublattice has been demonstrated, for the case of different symmetries of the magnetic order parameter over these sublattices. The symmetry analysis revealed that in *Re*OFeAs systems, there is no Heisenberg exchange between the spins of *Re* and Fe ions. The authors conclude that the magnetic *Re*–Fe interaction cannot be a substantial reason of the observed enhancement of T_c in the $ReO_{1-x}F_xFeAs$ compounds with magnetic *Re* ions.

2.2.3 Phase Diagrams

On doping of stoichiometric compounds possessing an SDW-type magnetic structure, their magnetic ordering temperature T_N decreases gradually, and a superconducting state sets on. The magnetic ordering is accompanied by structural distortion of the pristine (ideal) tetragonal phase, which turns into an orthorhombic one. It is of utter interest to trace the boundaries of all three phases – magnetic, structural and superconducting ones – in the (T, x) plane. In a rough approximation, the magnetic and the orthorhombic phases are coinciding on this plane, but it is

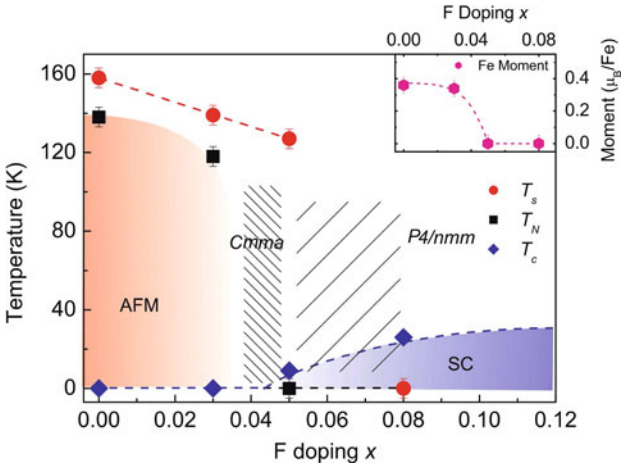

Fig. 2.19 Structural and magnetic phase diagram of $LaO_{1-x}F_xFeAs$, as determined from neutron experiments on the samples with $x = 0$; 0.03; 0.05; 0.08 [72]. In the inset, the x dependence of the mean magnetic moment per Fe atom, measured at 4 K, is shown

difficult to explore their borders in detail. Local methods, such as μSR or Mössbauer spectroscopy, provide information about long-range magnetic order, but they are not sensitive to structure distortions. On the other side, X-ray structure analysis accounts for the latter but neglects the magnetic ordering. There is only the neutron diffraction which allows to probe the both factors at the same time.

In [72], a detailed phase diagram of $LaO_{1-x}F_xFeAs$ has been obtained, based on the neutron diffraction analysis in combination of the traditional methods to study the superconducting state (Fig. 2.19). This publication extends the data obtained in [59, 73, 74] by neutron scattering, X-ray structure analysis, transport properties and μSR.

It is seen from Fig. 2.19 that magnetic and structural phase transitions occur in a narrow region of concentration x (shaded) around $x = 0.04$. A careful analysis shows that the superconductivity starts at x values still within the orthorhombic phase, in which, however, the long-range magnetic order does not exist anymore. The larger part of the concentration domain of existence of superconductivity does, however, fall onto the tetragonal phase. This observation is typical for many *Re*OFeAs compounds, whereas the fine details of the (T, x) phase diagram differ over systems. For example, Fig. 1.1 shows the phase diagram of $CeO_{1-x}F_xFeAs$ [12]. Different from the $LaO_{1-x}F_xFeAs$ system, the disappearance of magnetic ordering is gradual, and its existence region, along with that of the orthorhombic phase, does not overlap with the region of superconductivity. The phase diagram in question resembles those of cuprates.

A more delicate situation takes place in $SmO_{1-x}F_xFeAs$ [75–77]. In an early work [75], the phase diagram shown in Fig. 2.20 has been obtained. The temperature of SDW-type ordering does rapidly fall down with doping. A superconducting state

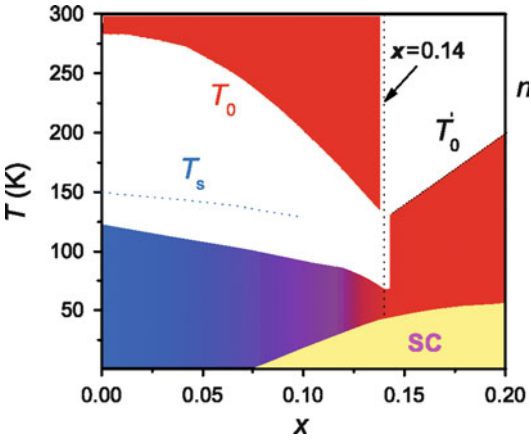

Fig. 2.20 Phase diagram of the $SmO_{1-x}F_xFeAs$ system [75]

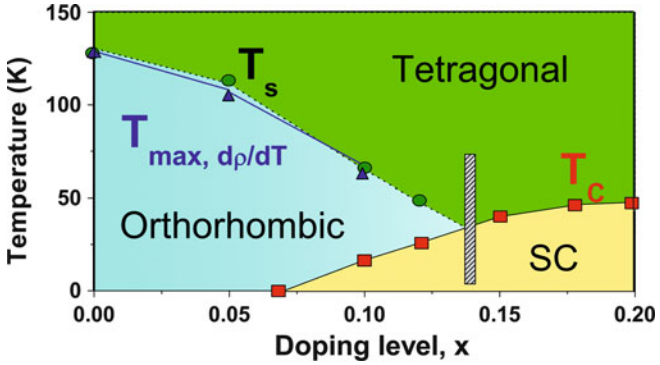

Fig. 2.21 Refined phase diagram of the $SmO_{1-x}F_xFeAs$ system [77]

appears at $x \sim 0.10$, passes through maximum of the transition temperature $T_c = 54$ K at $x = 0.20$ and further on does not change much. There exists a concentration region $0.05 < x < 0.15$ in which superconductivity and the SDW-type ordering do coincide. A more detailed study of the border of the region where both order parameters coincide needs yet to be better studied near the crossing of the lines $T_s(x)$ (dashed line in Fig. 2.20) and $T_c(x)$.

A possible coexistence of magnetic and superconducting order parameters in $SmO_{1-x}F_xFeAs$ has been addressed in [78]. The arguments in its favour come from μSR measurements for $x = 0.05$–1.0, in which region the $T_s(x)$ and $T_c(x)$ curves do overlap. This coexistence occurs at nanoscale, e.g. the domains of magnetic and superconducting phases do mutually disperse one into the other, having size of about 2 nm. This is exactly a typical coherence length of ξ in this compound. Such small-grain disperse coexistence does probably reveal a competition between magnetism and superconductivity in this compound.

In Fig. 2.21, a refined phase diagram of this compound is shown, from which it is clearly seen that superconductivity starts to grow inside the orthorhombic phase.

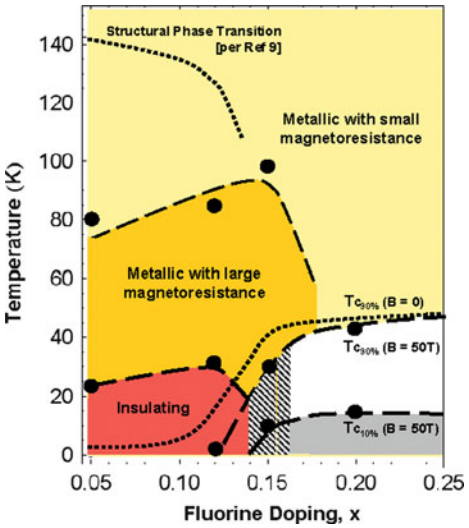

Fig. 2.22 Phase diagram of the $SmO_{1-x}F_xFeAs$ system in magnetic field of 50 T [76]

A shaded region around $x = 0.14$ marks the boundary between two different types of behaviour in the temperature dependence of electrical conductivity [77].

A further level of phase diagram detailing has been achieved in [76]. Figure 2.22 resumes the data on magnetoresistance; a region with large magnetoresistive effect is marked as shaded. At low levels of doping, a metallic phase with high magnetresistance persists, which, however, is replaced at low temperatures by a "dielectric" phase. The quotes mean that the electrical resistivity in this region varies with temperature as $\ln T$. The narrow shaded region at $0 < x < 0.14$ corresponds to the "dielectric" to metal transition. In the same region, a quite abrupt transition from orthorhombic into tetragonal phase takes place, in agreement with Fig. 2.21.

2.2.4 Magnetic Fluctuations

Fluctuations of the magnetic order parameter have effect onto the behaviour of magnetic susceptibility. We will consider here only the statical susceptibility $\chi(T)$ i its dependence on temperature. In Fig. 2.23, $\chi(T)$ over broad temperature range is shown for stoichiometric LaOFeAs [79]. Beyond the magnetic phase transition, $\chi(T)$ grows linearly, and notably this dependence is typical for FeAs-based systems. In the inset, the temperature dependence of the magnetic contribution in heat capacity, defined as $\partial(\chi_T)/\partial T$. As is seen, this latter property shows anomalies near the temperatures of magnetic (T_N) and structural (T_s) transitions. Particularly strongly do magnetic fluctuations reveal themselves near structure phase transition at $T_s = 156$ K (a sharp maximum in the $\partial(\chi_T)/\partial T$ curve).

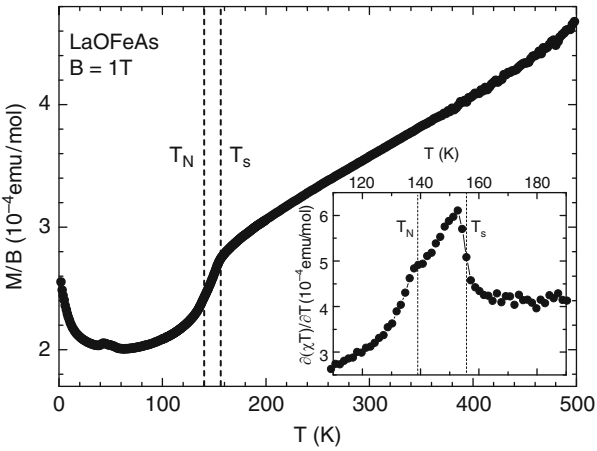

Fig. 2.23 Temperature dependence of magnetic susceptibility for LaOFeAs. In the inset: temperature dependence of the property $\partial(\chi_T)/\partial T$ in the vicinity of magnetic and structural phase transition [79]

In doped compounds, $\chi(T)$ does not change much up to concentrations $x < 0.04$, when superconductivity sets on, and for $T < T_c$ the magnetic susceptibility $\chi(T)$ exhibits a typically diamagnetic behaviour. Within the region of existence of superconductivity, up to $x < 0.125$, the slope of $\chi(T)$ in the normal (metallic) phase is only weakly x-dependent, i.e. $\chi(T)$ only slightly increases with temperature.

2.3 Electronic Structure

2.3.1 Stoichiometric Compounds

First-principles electronic structure calculation of the LaOFeP compound, in which superconductivity ($T_c = 4\,\mathrm{K}$) had been first found, was done prior to the discovery of high T_c values in this class of compounds [80]. Calculations for LaOFeAs have been done in fact independently by several groups [17,18,62,63,81–85]. We report here the results by Singh and Du [81], obtained by the augmented plane waves method (LAPW) within the local density approximation (LDA). In the calculation, the experimental values of the lattice parameters for LaOFeAs have been used: $a = 4.03552\,\text{Å}$, $c = 8.7393\,\text{Å}$. Internal coordinates of La and As atoms in the plane formed by Fe atoms were determined by minimization of total energy calculated in the LDA, yielding $z_{La} = 0.1418$, $z_{As} = 0.6926$. This resulted in the following inter-atomic distances: Fe–Fe 2.854 Å, As–As 3.077 Å, Fe–As 2.327 Å.

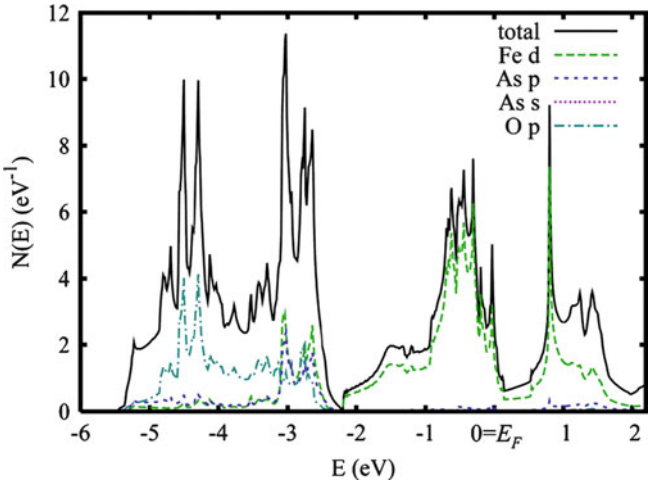

Fig. 2.24 Calculated density of states in LaOFeAs (*solid line*) and partial contributions to it from the orbitals of Fe, As and O (*dashed lines*) [81]

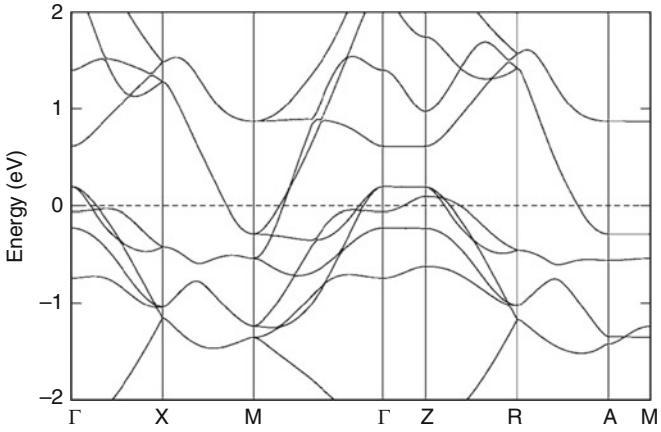

Fig. 2.25 Band structure of LaOFeP [80]

The calculated density of states (DOS) is shown in Fig. 2.24, where, along with the total one over unit cell, the partial contributions from Fed states, Op and Asp states are shown.

The Fermi energy cuts the region of Fed states which occupy the range from roughly -2 to $+2$ eV (assigning zero energy to the Fermi level). A broad region below the d states is formed by p states of As and O. The states of the La atoms fall into the range above the Fermi energy.

The band structure is shown in Fig. 2.25 taken from an earlier work by Lebeque [80] for the sole reason that the corresponding figure in [81] is complicated by

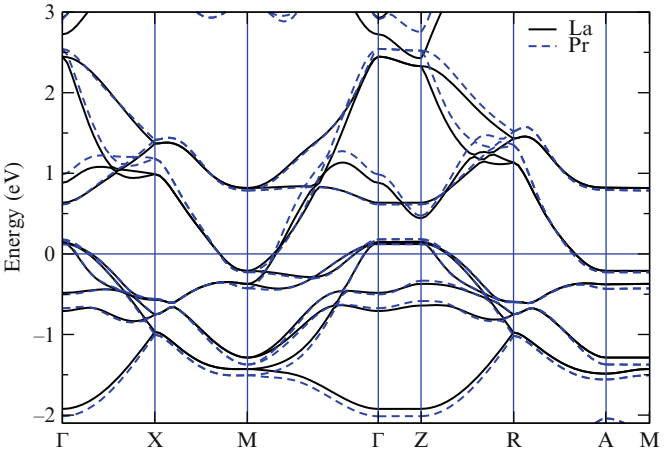

Fig. 2.26 Band structure of LaOFeAs (*solid line*) and PrOFeAs (*dashed line*), after [82]

additional data related to the variation of As coordinates in the lattice, whereas otherwise the results of [80] for LaOFeP are identical to those for LaOFeAs.

For a comparison, we show in Fig. 2.26 band structures calculated for two compounds, LaOFeAs and PrOFeAs, whose crystal structures are identical and lattice parameters are close to those of LaOFeP [82]. We see that the dispersion curves for the three compounds shown in Figs. 2.25 and 2.26 are qualitative identical, and quantitative differences tiny. A similarity between calculation results, even zoomed in a fine energy scale around the Fermi level, is maintained throughout the whole class of ReOFeAs-like compounds, so that Figs. 2.24 and 2.25 do faithfully represent all compounds of this type. In [82], a calculation through the series with Re = La, Ce, Sm, Nd, Pr, Y has been done and shown that there is practically no difference in the total DOS as well as in the details of the partial Fe3d states distribution.

The details of the dispersion of the bands crossing the Fermi level do determine the Fermi surface, which is multi-sheet in LaOFeAs compounds. The Fermi level crosses two hole bands centred at Γ and two electron bands emerging from M. Noteworthy is a flat character of curves along the Γ–Z direction, i.e. a weak dependence of hole quasiparticles' energy on the k_z momentum, so that the Fermi surface around Γ has cylindrical shape. The same observation applies to the sheets of the Fermi surface in the vicinity of M (as follows from the flat dispersion of the electron bands along the M–A line).

Therefore, the Fermi surface of the LaOFeP compound contains two hole cylindrical sheets with the axis along Γ–Z and two electron ones along M–A. This reveals a quasi-two-dimensional character of electronic states, formed by d_{xz} and d_{xy} orbitals. Beyond the said four cylindrical sheets, a three-dimensional hole pocket is present, centred at Z (see Fig. 2.27) and formed by the Fed states, hybridized with p states of As and La.

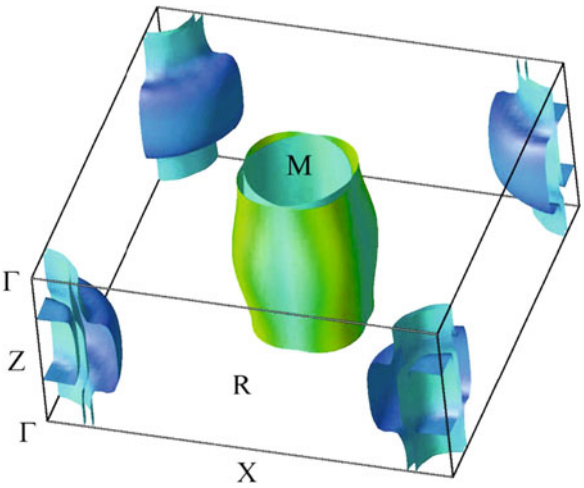

Fig. 2.27 Fermi surface of LaOFeAs [81]. Symmetry points of the Brillouin zone: Γ (0,0,0), Z (0,0,1/2), X (1/2, 0,0), R (1/2.0,1/2), M (1/2,1/2,0) in the units of $2\pi/a$

Three hole sheets, taken together, make 80% of the state density $N(E_F)$ at the Fermi level. The average electron velocity on them, taken in the xy plane, is $0.81 \cdot 10^7$ cm s^{-1}. The corresponding numbers for two electron sheets are $2.39 \cdot 10^7$ and $0.37 \cdot 10^7$ cm s^{-1}. From here, a high anisotropy of conductivity (of about 15) follows, which again underlines a quasi-two-dimensional character of electron states in this material.

The summary volume confined within two electron cylinders (and equal to the volume within the hole cylinders) is 0.13 electrons per formula unit. The value of the density of states (per formula unit and both spin components) is $N(E_F) = 2.02\,(\text{eV})^{-1}$. Hence, LaOFeAs is a conductor with low carrier concentration and relatively high density of states on the Fermi level, quite differently from the situation in cuprates.

Numerous calculations of electronic structure for different LaOFeAs-type compounds give quite similar results: flat regions in the dispersion curves around the Fermi level along Γ–Z and M–A, which yield hole and electron cylindrical sheets of the Fermi surface and reveal quasi-two-dimensional character of electronic states in the FeAs layers.

Let us now turn more attentively to the structure of Fe3d states, which play a major role in the formation of electronic properties of FeAs-type compounds, since, namely, these states are pronounced at the Fermi level. In a free Fe ion, the fivefold degenerate 3d term includes five orbitals – d_{xz}, d_{yz}, d_{xy}, $d_{x^2-y^2}$ and $d_{3z^2-r^2}$, – whose wave functions are shown in Fig. 2.28. The d_{xz} and d_{yz} orbitals each have four lobes, positioned in the xz and yz planes, correspondingly. The d_{xy} and $d_{x^2-y^2}$ orbitals are in the xy plane, with the difference that the lobes of $d_{x^2-y^2}$ are directed along the x and y axes, whereas in the d_{xy} – along the diagonals of the quadrants,

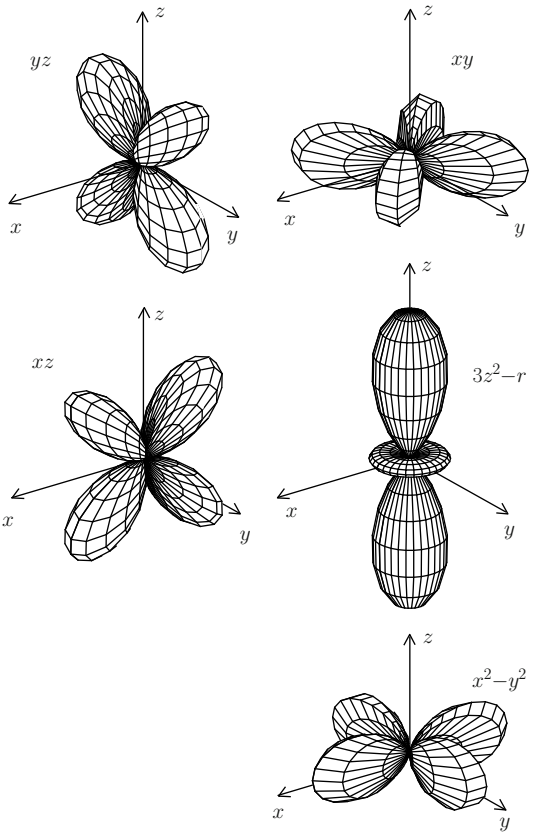

Fig. 2.28 Graphical representation of five degenerate orbulals for $3d$ electrons of the Fe ion

i.e. rotated by 45°. Finally, the $d_{3z^2-r^2}$ orbital has one lobe directed along the z axis, complemented by a z-axial symmetric structure in the xy plane.

In cubic-symmetry crystal field, the fivefold degenerate $3d$ level splits into the e_g doublet and t_{2g} triplet, which correspondingly include the following orbitals:

$$e_g : \left(d_{3z^2-r^2},\ d_{x^2-y^2}\right); \quad t_{2g} : \left(d_{xz},\ d_{yz},\ d_{xy}\right). \tag{2.2}$$

In the structure of LaOFeAs, each Fe ion is surrounded by four As atoms, which form a distorted tetrahedron. In tetrahedral crystal field, the t_{2g} level is situated lower in energy than the e_g one.

For a more convenient discussion on the LaOFeAs crystal structure, it is more convenient to rotate the coordinate system by 45° around the z axis, which results in interchanging the $d_{x^2-y^2}$ and d_{xy} orbitals, so that the attribution into e_g and t_{2g} groups becomes as follows:

$$e_g : \left(d_{3z^2-r^2},\ d_{xy}\right); \quad t_{2g} : \left(d_{xz},\ d_{yz},\ d_{x^2-y^2}\right). \tag{2.3}$$

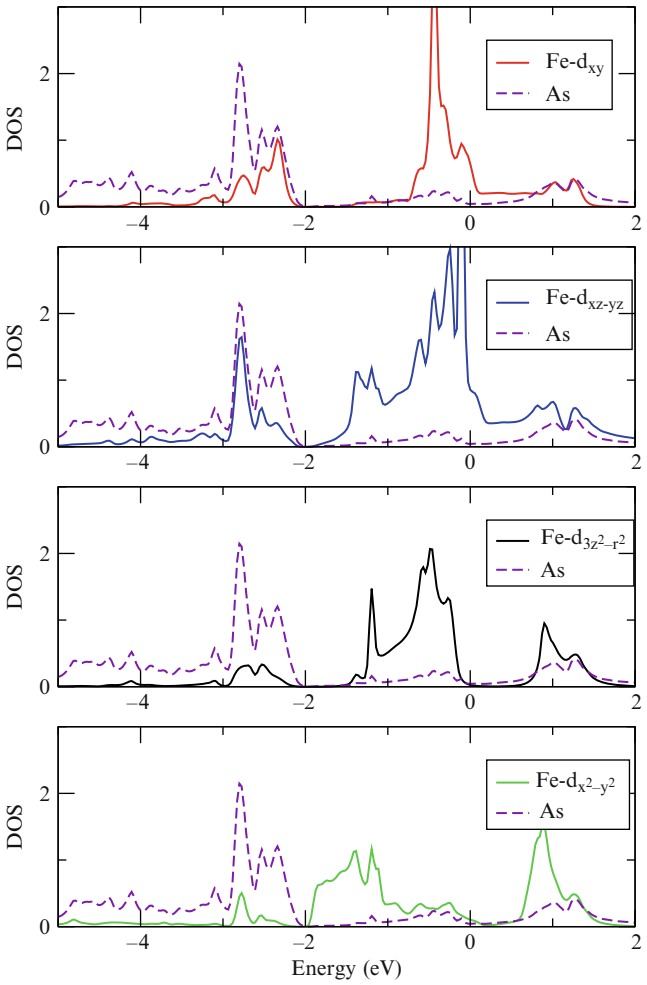

Fig. 2.29 Partial densities of states of the Fe-d orbitals (*solid lines*) and As-p orbitals (*dashed lines*), after [85]

This is the setting traditionally used in the description of electronic properties of the FeAs-type compounds.

Partial contributions of different orbitals into the total Fe3d density of states were calculated in [85] for LaOFeAs, see Fig. 2.29. It follows from Fig. 2.29 that the d_{xz}, d_{yz} and d_{xy} orbitals have a considerable weight in the energy range from -3 to -2 eV, where the contributions of the Asp orbitals are concentrated. An overlap of the said Fed orbitals with the Asp orbitals results in their large hybridization, which ensures an efficient hopping of d electrons over Fe sublattice to next-nearest neighbours, via intermediary As ions.

2.3.2 The Role of Magnetic Ordering and Doping

The results shown in Figs. 2.24–2.29 refer to paramagnetic stoichiometric compounds. At low temperatures, the SDW-type ordering takes place which influences on the electronic structure, – dispersion curves and density of states. The other relevant problem is the calculation of the electron spectrum of doped systems. It can be a priori expected that the electron doping is about to enlarge the electron pockets of the Fermi surface, and the hole doping – the hole pockets. However, to figure out how precisely does this happen, calculations are needed for compounds with a given (controllable) level of doping.

Doped systems, e.g. $LaO_{1-x}F_xFeAs$, are disordered in what regards the distribution of F ions over the LaO sublattice. A modelling of such systems poses a theoretical problem, which demands to adopt some approximative treatment. In practice, two approaches are largely accepted: the virtual crystal approximation and the supercell approach, i.e. a substitution of a disordered crystal, at some special level of doping, by an ordered one, immediately including dopant at some sites. For example, the situation $x = 0.125 = 1/8$ can be imitated by an 8× enlarged supercell, in which one of eight oxygen atoms is replaced by fluorine. The translation symmetry thus restored, a calculation can be done by a standard band-structure technique, in an assumption that its results would faithfully enough reproduce the expected behaviour of the disordered structure for the x given. The above value of $x = 0.125$ is indeed very common for many doped LaOFeAs systems, since it is close to this level of doping that the superconducting state sets on.

Let us discuss the first works in which the both problems – the SDW-type ordering and doping – are addressed simultaneously [86]. Figure 2.30 shows the band structure of stoichiometric LaOFeAs along with that doped with fluorine ($x = 0.05$), for non-magnetic case. The curves 1, 2 and 3 correspond to the hole-type spectrum of quasiparticle states, and the curves 4 and 5 to the electron-type one. It can be seen from the figure that the fluorine doping decreases the hole pockets and

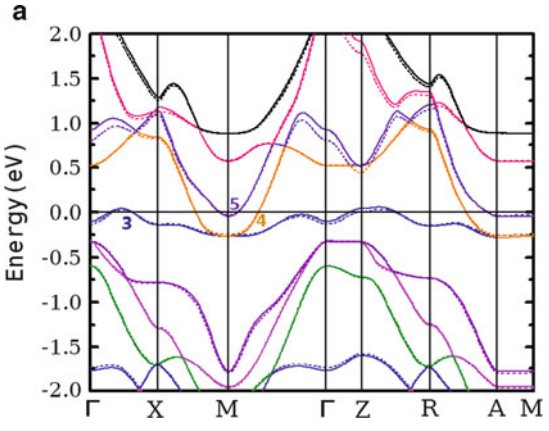

Fig. 2.30 Calculated band structure of the nonmagnetic compound $LaO_{1-x}F_xFeAs$ for stoichiometric composition (*solid line*) and under fluorine doping (*dotted line*) ($x = 0.05$) [86]

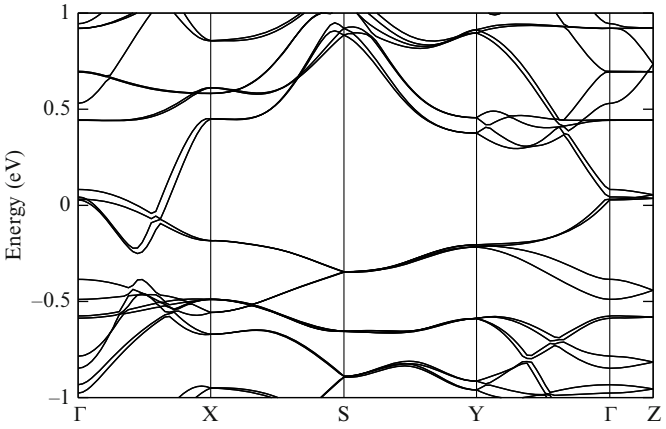

Fig. 2.31 Band structure of LaOFeAs in its magnetically ordered phase with the wave vector $\mathbf{q}_M$, taking the orthorhombic distortion into account. Symmetric points of the Brillouin zone: Γ (0,0,0), S (1/2,1/2,0), Y (0,1/2,0) and Z (0,0,1/2) [88]

increases the electron ones. Therefore, the fluorine doping does, indeed, correspond to electron doping that is confirmed by the sign of the Hall coefficient. It is reported in [86] that an increase of x leads to a further extension of the electron pockets.

The band structure of magnetically ordered phase has been addressed in [84, 86–88]. It was shown that both the antiferromagnetic (AFM) and the SDW phases are energetically preferable over the nonmagnetic one. In the last of these works [88], the true SDW-type magnetic ordering found in the FeAs-type compounds has been considered, namely a stripe magnetic structure with antiferromagnetic alteration of chains in the basal plane and along the z axis, described by the wave vector $\mathbf{q}_M$.

In Fig. 2.31, calculated energy dispersion curves along symmetry directions of the orthorhombic Brillouin zone are shown after [88]. The resulting picture is very close to that obtained for the SDW-type structure with ferromagnetic ordering of chains, instead of their alternation, along the z axis, so that the third component of the wave vector $\mathbf{q}_M$ be zero. This similarity is explained by the smallness of exchange interaction between adjacent FeAs layers, due to a quite large separation of the latter.

As can be seen from a comparison of Fig. 2.31 with Fig. 2.25 for non-magnetic case, the magnetic ordering does substantially alter the band spectrum. A broad gap between the valence and the conduction bands appears over almost the whole Brillouin zone, and is also revealed as a pseudogap in the density of states. The Fermi level is crossed by four dispersive bands close to Γ, at some points along the Γ–X line. The hole sheets have the shape of narrow cylinders due to the presence of a flat region in the dispersion curves along the Γ–Z. The electron sheets are more deformed along the c axis.

The density of states for magnetically ordered crystal is shown in Fig. 2.32, where along with the results for the stoichiometric compound, the calculations for two

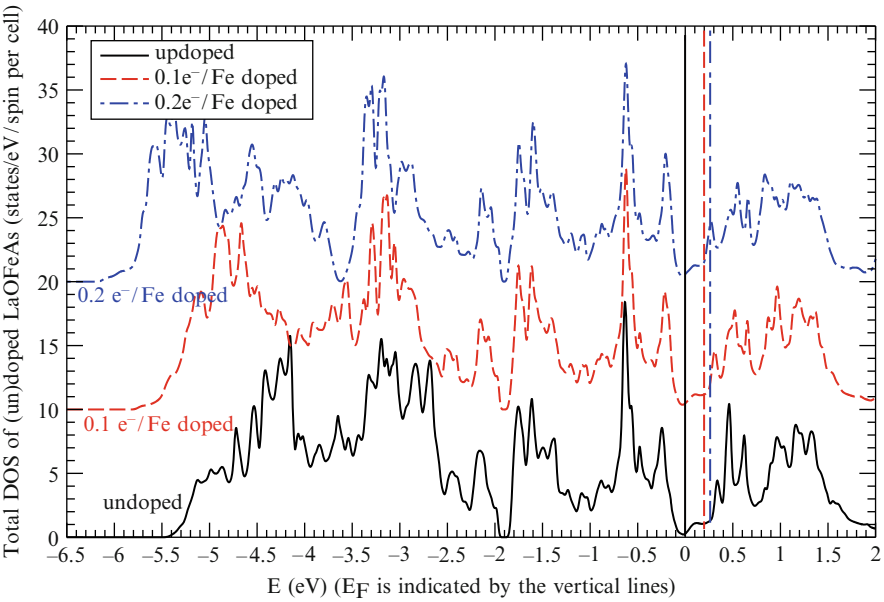

Fig. 2.32 Density of states in magnetically ordered LaOFeAs compound, nondoped and electron-doped to 0.1 and 0.2 electrons per Fe atom. For convenience, the *curves* are shifted one with respect to the other by 10 units along the ordinate axis [88]

electron-doped ones are presented [88]. It is seen that the Fermi level falls into the pseudogap; however, in the range where the density of states is dominated by Fe*d*, it is hardly affected by doping. This is a consequence of the virtual crystal approximation used, i.e. in fact, the rigid-band approximation. In reality, as is known from experiment, at such level of doping as $x = 0.2$, the SDW-type ordering does not survive. To grasp this effect, it is necessary to go beyond the LDA and take electron correlations into account, as will be described in Chap. 4.

An effect of external pressure on the electronic structure is shown in Fig. 2.33. Along with the changes in the energy dispersion curves, the density of states is affected. Specifically, the first peak above E_F shift towards the Fermi level, but the peak below E_F, in the interval 0.1 eV downwards, rests practically unchanged. Consequently, the pressure must induce changes in superconducting properties of electron-doped materials, whereas the expected effect onto the properties of hole-doped ones should be less important.

The results of the LDA calculations are shown in Fig. 2.33 used relative positions of As atoms (i.e. z_{As} parameters) as obtained by total energy minimization (relaxation procedure). The importance of this procedure is illustrated by Fig. 2.34 and Table 2.2 [88].

At all values of z_{As}, the total energy of the $\mathbf{q}_M$ (SDW)-phase is the lowest one in relation to the ferromagnetic and antiferromagnetic phases. The magnitude of the magnetic moment in the SDW phase is substantially lower at the optimized value

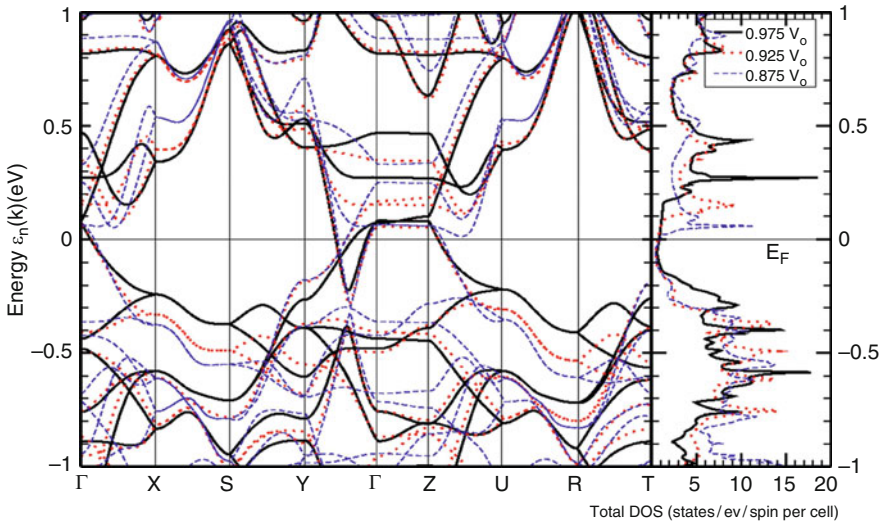

Fig. 2.33 Band structure of magnetically ordered LaOFeAs compound, calculated at different volumes: 0.975 V_0, 0.925 V_0 and an applied pressure. In the *right panel*, the density of states at different volumes is shown [88]

Table 2.2 Calculated electronic structure of compounds. The sheets of the Fermi surface are indicated: $h(\Gamma)$ and $h(Z)$ – the hole ones, centred at Γ and Z points, respectively; $e(M)$ – electron ones, centred near the M point of the Brillouin zone

Compound	Fermi surface	References
LaOFeAs	$2h(\Gamma), h(Z), 2e(M)$	[17, 18, 37, 62, 81, 84, 85]
LaOFeAs	$h(Z)$ absent, *APM*	[63]
LaOFeP	$2h(\Gamma), h(Z), 2e(M)$	[80]
LaOFeP	*ARPES*:$h(\Gamma), e(M)$	[92]
NdOFeAs	*ARPES*:$h(\Gamma), e(M)$	[93]
LaONiP	$h(X), 3e(M)$	[93]
LaONiAs	$h(X), 2e(M)$	[37]
*Re*OFeAs *Re* = La,Ce,Sm,Nd,Pr,Y)		[82]

of z_{As} than in experiment. The differences of the values listed in the last column for spins ↑ and ↓ do exactly yield the magnitude of the magnetic moment shown in the first column.

The comparison of the second and the third lines in the Table 2.2 reveals that the numerical results are quite sensitive to the calculation scheme adopted. It is moreover noteworthy that in the above cited work [88] further factors affecting the calculation results are cited. Moreover, this work covers the results related to a substitution of As by other elements (P, Sb, N), as well as La substitution by other rare-earth elements.

A comparison of results obtained by different groups and with different calculation techniques does often reveal some disagreements – minute ones in what

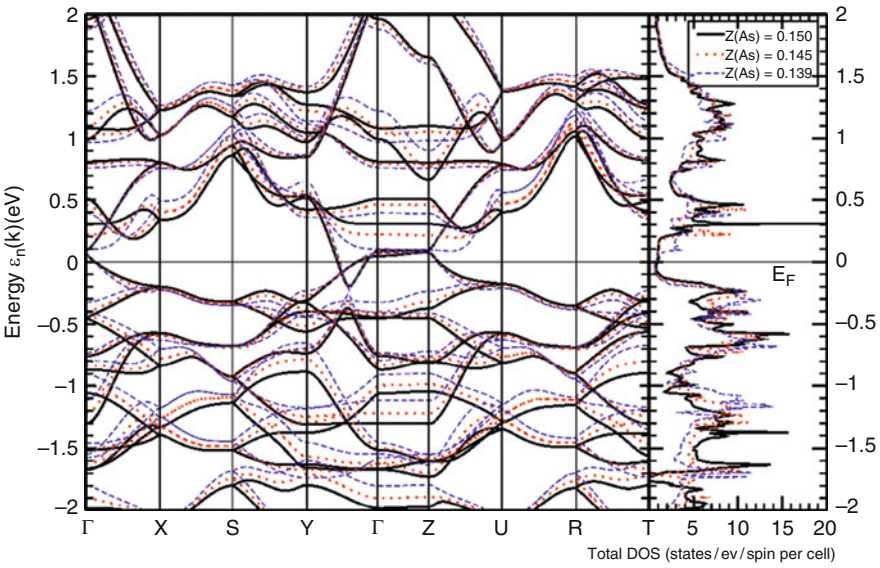

Fig. 2.34 Band structure of magnetically ordered LaOFeAs, calculated for different values of the z_{As} parameter: 0.150, 0.145, and 0.139 [88]

regards the band structure and the Fermi surface, yet sometimes contradictory in relation to magnetic properties and, in particular, the magnetic ground state of the FeAs-type systems. Since the discovery of superconductivity, calculations of the pristine compound LaOFeAs have been reported, which predict both ferromagnetic and antiferromagnetic structures, moreover the latter one of both chessboard-like and stripes-like types, as the ground state. The smallness of the energy differences between the structures is due to itinerant character of magnetism in the FeAs-type systems, extremely sensitive to the details of their electron and crystalline structure and, in particular, to the precise positioning of the As atoms, given by the z_{As} parameter. In [90], four different methods (two all-electron ones and two pseudopotential ones) have been used to calculate all electronic properties of the LaOFeAs compound, and the conclusions drawn about the abilities and accuracy of each method. Thus, for the analysis of magnetic properties, e.g. the calculation of magnetic phase diagrams, an LDA calculation with theoretically determined z_{As} parameters could have been recommended, how it has been used, e.g. in [91].

2.3.3 Experimental Studies of the Fermi Surface

There are two methods of experimental determination of the Fermi surface in metals, one based on the de Haas–Van Alphen (dHvA) effect, the other on the angle-resolved photoelectron spectroscopy (ARPES). In the first case, an information

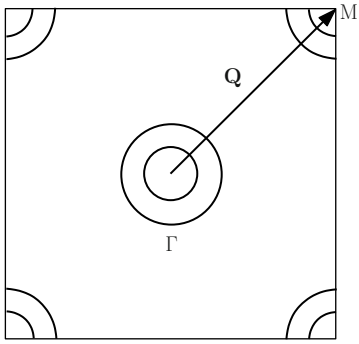

Fig. 2.35 Schematic representation of the Fermi surface in the *Re*OFeAs compounds

about cross-sections of the Fermi surface is extracted from detected fluctuations of magnetization as function of the magnetic field. This method is very accurate but it does not relate the measured cross-section to its actual placement in the **k**-space of the Brillouin zone. ARPES has inferior accuracy but permits a direct recovery of the Fermi surface in the **k**-space. Hence, both methods have advantages and shortcomings and are, in practice, complementary.

LDA calculations of ReOFeAs compounds and other isomorph compounds, e.g. LaOFeP, exhibit a common structure of the Fermi surface. It consists of two cylindrical hole pockets, which include the Brillouin zone centre, two electron pockets centred at the Brillouin zone corners and, moreover, a three-dimensional hole pocket around Γ. A $k_z = 0$ section of such multi-sheet Fermi surface is shown in Fig. 2.35.

The **Q** vector connecting the Γ and M points is close to the nesting vector which connects congruent points of the hole and electron pockets of the Fermi surface, since the sizes of these pockets, according to LDA calculations, are almost identical. The nesting determines the details of magnetic susceptibility of these compounds, in particular, the SDW magnetic structure, as will be shown in Chap. 4.

An experimental verification of these conclusions has been done with the use of ARPES [92, 93]. Thus, in [93] the ARPES spectra of the $NdO_{1-x}F_xFeAs$ single crystal have been measured, which indicated the pockets of the Fermi surface around Γ and M points of the Brillouin zone (Fig. 2.36), in agreement with first-principles calculations.

In [92], the measured PES of the LaOFeP compound, integrated over angles, enabled to recover the density of states over the broad energy interval, which comes out in agreement with numerical calculations. Angle-resolved measurements of photoemission detected two sheets of the Fermi energy around the Γ point along with a further sheet (apparently a degenerate one) around the M point. The works cited let us to conclude that the main features of calculated electronic structure of the LaOFeAs-type compounds have found experimental confirmation.

In parallel, first work on the study of the Fermi surface using the dHvA effect have appeared [94, 95]. The study was done for the LaOFeP compound whose crystal structure is the same as of LaOFeAs, and the superconducting transition temperature is $T_c \sim 7\,\mathrm{K}$. This choice was motivated by a need of a high-purity

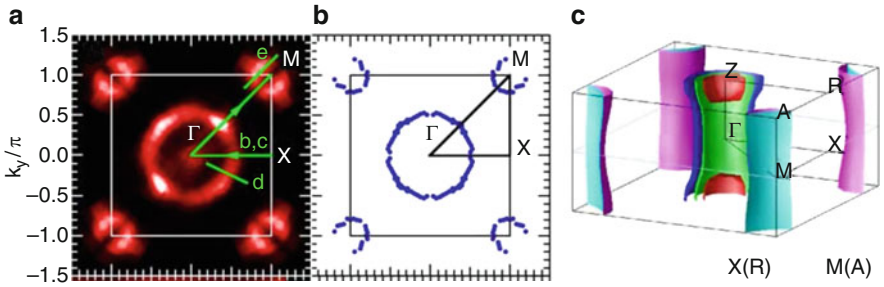

Fig. 2.36 Pockets of the Fermi surface, reconstructed from ARPES measurements on an $NdO_{1-x}F_xFeAs$ single crystal (**a**–**b**), and their comparison with the Fermi surface calculated within the LDA (**c**) [92]

single crystal sample with not so high value of the upper critical field ($H_{c2} \approx 0.68$ T for $B_{\parallel c}$ and 7.2 T for $B_{\perp c}$), to be able to suppress superconducting state by an experimentally readily accessible field. The results have shown that this compound has two cylindrical hole surfaces, centred at Γ, and two electron ones, centred at M. Hence, a full agreement with the LDA results by Lebeque [80] was found, albeit with higher effective masses, of 1.7–2.1 m_e (m_e: free electron mass), instead of about 0.8 m_e as calculated. Therefore, the main conclusions of the LDA calculations for FeAs-type systems found experimental verification on the basis of different methods.

A detailed comparison of LDA calculation results with the ARPES data revealed certain discrepancies. Thus, in [96] a thorough analysis of electron spectra of two stoichiometric compounds LaOFeP and LaOFeAs has been done (Fig. 2.37). In the (a) panel, around Γ two hole pockets Γ_1 and Γ_2 are seen, and an electron pocket – near the M point. In LaOFeP, they include, correspondingly, 1.94 holes, 1.03 holes and 0.05 electrons. For LaOFeAs, the corresponding numbers are 1.86 and 1.18 (Γ_1 / Γ_2); the electron M pocket is difficult to measure because of its peculiar cross-like shape. We note in addition that the inner (Γ_1) pocket in both compounds is doubly degenerate, as well as the M-centred electron one. Therefore, the Fermi surface consists of five sheets ($2 \times \Gamma_1 + \Gamma_2 + 2 \times M$), exactly as the LDA calculations for both compounds predict it to be.

A detailed comparison of LDA calculations with ARPES data [96] reveals a good agreement between theory and experiment, which is further confirmed by recent studies of the dHvA effect [95] on LaOFeP. For the other compound, LaOFeAs, the agreement between ARPES and LDA calculations is worse (a presence of the cross-shaped pocket at M, not predicted in the calculations). As of now, the reason for such disagreements is not clear. Taking into account the situation with other compounds of the ReOFeAs group, one can conclude about the agreement between LDA calculations and experimental data only in what regards the main result, the number and approximate size of electron and hole pockets; the fine details of electronic structure may differ.

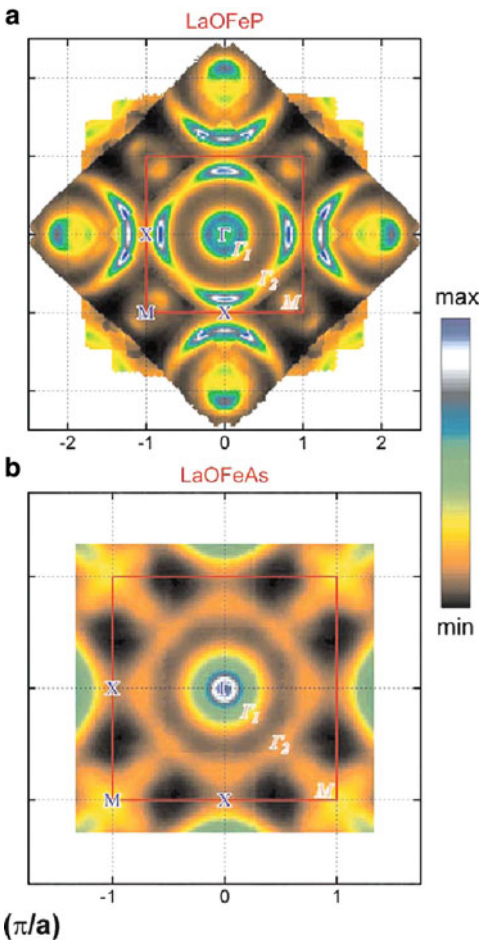

Fig. 2.37 Map of the Fermi surface of two compounds LaOFeP (**a**) and LaOFeAs (**b**), obtained from symmetrized ARPES data [96]

2.4 Symmetry of the Superconducting Order Parameter

2.4.1 Experimental Methods of Determining the Order Parameter

A knowledge of the symmetry and the shape, in the momentum space, of the superconducting order parameter (gap in the electron spectrum at the Fermi surface) is of particular importance, since it allows to make conclusion about the pairing mechanism. Several scenarios have been suggested for explaining the mechanism of superconductivity in the new class of superconductors, corresponding to different predictions for the symmetry of the order parameter: s, p or d type. There are several ways to determine experimentally the superconducting gap, and, consequently, to study the symmetry of the superconducting order parameter.

One of such methods is nuclear magnetic resonance (NMR), in which the Knight shift and the spin–lattice relaxation rate are measured. From the temperature dependence of the one and the other, information about superconducting order parameter can be gained.

Particularly informative in this sense are spectroscopic methods, in which the current I is measured as function of the voltage applied to the sample and the conductance dI/dV is determined; further on, the superconducting gap is found by adjustment of experimental curves to theoretical ones. The methods which fall within this group are: scanning tunnel spectroscopy (STS), photoelectron spectroscopy (PES), angle-resolved photoelectron spectroscopy (ARPES), point contacts with Andreev reflection (PCAR). In these methods, the density of quasiparticle states in a superconductor is directly measured. Immediately close to these methods is the Josephson contact spectroscopy.

There are also methods of different types: from measurement of the temperature dependence of the penetration depth of magnetic field into a superconductor, $\lambda(T)$. Moreover, certain information about the symmetry of superconducting order parameter can be gained from temperature dependence of electronic specific heat $C_v(T)$.

The whole spectrum of these methods has been applied to *Re*OFeAs compounds doped with different elements yielding them superconducting. The results of these studies are summarized in Table 2.3. In the following, we describe these results in detail, grouping them according to the methods used.

2.4.2 Nuclear Magnetic Resonance

Measurements of the resonance frequency and linewidth of the NMR at ^{57}Fe and ^{75}As nuclei make it possible to extract important information on electronic and magnetic properties of the FeAs-type systems. This information is contained in two characteristics immediately measurable in the NMR: the Knight's shift K and the spin–lattice relaxation rate $1/T_1$. The latter is expressed from the imaginary part of the dynamic electron susceptibility $\chi(\mathbf{k}, \omega)$ via a well-known relation:

$$1/T_1 \sim |A_{nf}|^2 \sum_{\mathbf{k}} \frac{\mathrm{Im}\,\chi(\mathbf{k}, \omega_0)}{\omega_0}, \tag{2.4}$$

where ω_0 is the NMR frequency, and A_{nf} – the constant of hyperfine interaction, coupling the nuclear spin of an isotope to the conductivity electrons.

Since ω_0 is small against characteristic electron-related frequencies, including kT_c, the $1/T_1$ property is determined by low-frequency density of states in the spectrum of spin fluctuations in the electron system. Due to a presence of a gap on the Fermi surface of a superconductor, $\mathrm{Im}\,\chi(\mathbf{k}, \omega_0)$ is exponentially small for $T < T_c$, which in its turn leads to an exponential dependence of $1/T_1$ upon temperature in

Table 2.3 Superconducting order parameter in the *Re*OFeAs compounds, according to the data obtained by different methods.

Compound	T_c, K	Experiment	Order parameter	Reference
$LaO_{0.7}FeAs$	28	NMR	$1/T_1 \sim T^3$	[99]
$LaO_{0.92}F_{0.08}FeAs$	23	NMR	d or s, $\Delta_1 = 4\,kT_c$, $\Delta_2 = 1.5, kT_c$	[100]
$LaO_{0.89}F_{0.11}FeAs$	28	NMR	Pseudogap	[101]
$LaO_{1-x}F_xFeAs$ $0.04 \leq x \leq 0.14$	–	NMR	$1/T_1 \sim T^3$, pseudogap	[102]
$LaO_{1-x}F_xFe_{0.95}Co_{0.05}As$	–	NMR	Differs from $1/T_1 \sim T^{2.5-3}$ and exponent	[103]
$LaO_{0.9}F_{0.1}FeAs$	26	NMR	$1/T_1 \sim T^3$, pseudogap	[98]
$LaO_{1-x}F_xFeAs$	27	PCAR	$\Delta = 2.8$–4.6 meV,s-type, pseudogap	[126]
$LaO_{0.9}F_{0.1}FeAs$	28	PCAR	$\Delta = 3.9$ meV, *ZBP*	[104]
$SmO_{0.85}F_{0.15}FeAs$	42	PCAR	$\Delta = 6.67$ meV, s-type	[105, 106]
$SmO_{0.85}FeAs$	52	STS	$\Delta = 8$ meV, *ZBP*	[108]
$SmO_{0.9}F_{0.1}FeAs$	51.5	PCAR	$\Delta_1 = 10.5$ meV, $\Delta_2 = 3.7$ meV, *ZBP*	[109]
$SmO_{0.8}F_{0.2}FeAs$	49.5	TRS	$\Delta = 8$ meV, pseudogap $\Delta_{GP} = 61 \pm 9$ meV	[112]
$NdO_{0.9}F_{0.1}FeAs$	–	PCAR	$\Delta_1, \Delta_2.ZBP$	[113]
$NdO_{0.9}F_{0.1}FeAs$	–	$\lambda(T)$	Δ, s-type	[114]
$NdO_{0.9}F_{0.1}FeAs$	53	ARPES	$\Delta = 15$ meV, s-type	[111]
$NdO_{0.86}F_{0.14}FeAs$	48	STS	$\Delta = 9.2$ meV, pseudogap, s-type	[110]
$NdO_{0.85}FeAs$	52	PES	Gap on the electron M-surface	[115]
$NdO_{0.9}F_{0.1}FeAs$	43	$\lambda(T)$	Two gaps, $\Delta\lambda \sim T^2$	[107]
$PrO_{0.89}F_{0.11}FeAs$	45	NMR	$1/T_1 \sim T^3$, $\Delta_1 = 3.5\,kT_c$, $\Delta_2 = 1.1\,kT_c$	[97]
$PrO_{1-y}FeAs$	35	$\lambda(T)$	$\Delta/kT_c \geq 1$	[116]

the superconducting state and results in an appearance of the Hebel–Slichter peak in the vicinity of T_c.

The above is valid if the superconductor gap does not become zero on the Fermi surface, e.g. in case of s symmetry of the superconducting order parameter. If the superconducting gap has zeros in some points or along certain lines on the Fermi surface, then the $1/T_1$ property, and also electron specific heat, do exhibit temperature dependence in the form of power law:

$$1/T_1 \sim T^n, \tag{2.5}$$

with some n value. For a two-dimensional system in the case of, say, d symmetry of the order parameter, $1/T_1 \sim T^3$. From measurements of spin–lattice relaxation in a superconductor, one can judge about the symmetry of the order parameter or at least draw conclusions on whether the superconductor gap has zeros on the Fermi surface.

If the gap Δ has no zeros on the Fermi surface, it can be extracted from the experimental data on $1/T_1$ using the relation following of the BCS theory:

$$\frac{T_{1,N}}{T_{1,S}} = \frac{2}{kT} \iint N_S(E) N_S(E') [1 - f(E')] \delta(E - E')\, \mathrm{d}E\, \mathrm{d}E', \tag{2.6}$$

or a correspondingly more involved expression for the case when the superconductor has two gaps on different sheets of the Fermi surface. Here, $T_{1,\mathrm{S}}$ and $T_{1,\mathrm{N}}$ stand for spin–lattice relaxation times in superconducting and normal phases of a metal, correspondingly, and $N_\mathrm{S} = \frac{E}{\sqrt{E^2-\Delta^2}}$ is density of states in the superconducting state.

An information concerning the gap can as well be extracted from the Knight shift which, in the BCS theory, can be expressed as follows [97]:

$$\frac{K_\mathrm{S}}{K_\mathrm{N}} = \int N_\mathrm{S}(E)\frac{\partial f(E)}{\partial E}\mathrm{d}E. \tag{2.7}$$

In the last formula, $f(E) = (1 + e^{E/kT})^{-1}$ is the Fermi function. Hence from measurements of $1/T_1$ one can judge about the presence of zeros of the gap on the Fermi surface. If such zeros do not come about, a comparison of experimental data on the Knight shift with model calculations results permits to extract the gap value.

NMR studies of superconducting FeAs-type compounds have been done in a number of works [97–103], with the results collected in Table 2.3. It is seen that in many cases, a power-law behaviour is detected. It is moreover remarkable that in no system was the Hebel–Slichter coherent peak detected. Joint data on the temperature dependence of $1/T_1$ are shown in Fig. 2.38.

For most of the FeAs-compounds, the power law close to T^3 is observed, however in the $LaO_{0.89}F_{0.11}FeAs$ sample studied in [103], the behaviour of $1/T_1$ is

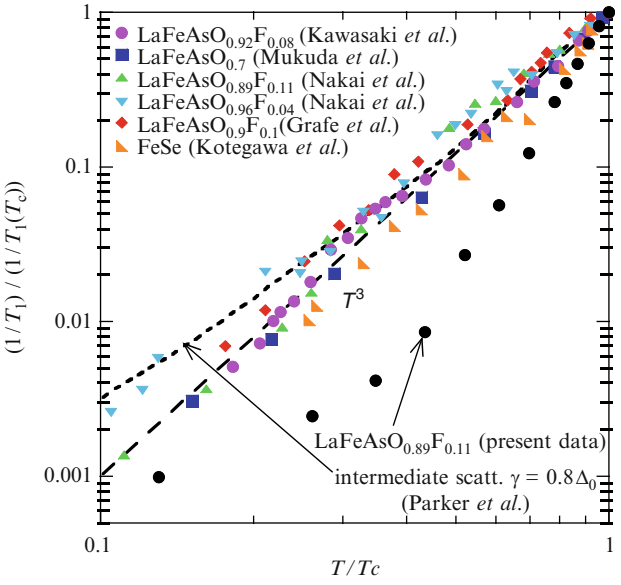

Fig. 2.38 Temperature dependence of the spin–lattice relaxation rate $1/T_1$ for a number of superconducting $LaO_{1-x}F_xFeAs$ compounds [103]

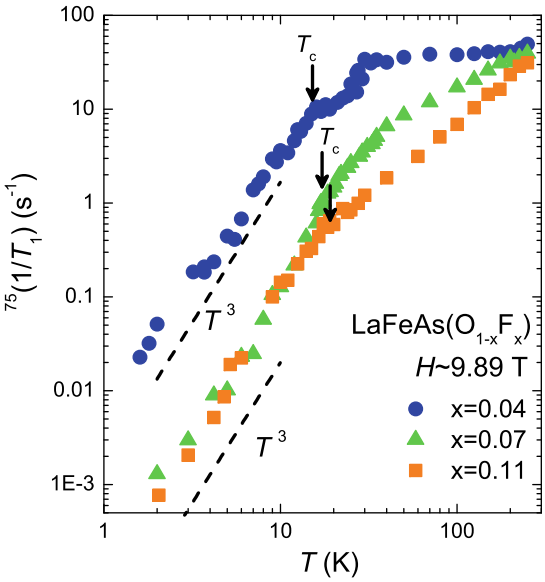

Fig. 2.39 Temperature dependence of $1/T_1$ in the $LaO_{1-x}F_xFeAs$ system at different levels of doping [102]

more complicated. At $T > 0.5\,T_c$, the $1/T_1$ follows the temperature rather as $\sim T^6$, and at even lower temperatures no power-law behavior is seen at all.

Systematical studies on the same system $LaO_{1-x}F_xFeAs$ over broad interval of doping ranges have shown that the power law stands – see results in [102] shown in Fig. 2.39. In the same work, devoted to measurements of $1/T_1$ over broad temperature ranges, for $x > 0.11$ a pseudogap Δ_{PG} of the order of kT_s, $T_s \sim 150\,K$ being about the temperature of magnetic transition in non-doped compound, has been detected above T_c. A presence of pseudogap in the spectrum of quasiparticle states in the normal phase of a superconductor is typical for cuprates where, as it is well established by now, it appears due to interaction of electrons with spin fluctuations. Among the FeAs-type systems, the presence of a pseudogap has been confirmed, by NMR and other methods, in a number of compounds – see Table 2.3.

Now, an important comment can be in place. An observation of the power-law behavior of $1/T_c$ does not yet mean that in a superconductor given, a gap is realized with zeros somewhere on the Fermi surface. One should take into account that in the FeAs-type systems, the Fermi surface is a multi-sheet one; hole-like around Γ and electron-like around M. On both hole and electron sheets, an s-type superconducting state (that without zero gap) can emerge; however, the signs of the gap function on these sheets may either coincide or be inverse. In case of sign coincidence one talks of extended s symmetry of the order parameter, whereas the opposite signs are referred to as the $s^{\pm}$ symmetry. In [90, 117], an idea has been put forward that in the FeAs-type systems, namely the $s^{\pm}$ symmetry of the order parameter is realized. This idea turned out to be very fruitful (see Chap. 4) and allowed to explain the power-law temperature dependence of $1/T_1$ in a different way.

When considering the gaps on the hole and electron sheets of the Fermi surface in the **k**-space, then obviously on a transition from hole to electron sheet, in case of $s^{\pm}$ symmetry, the gap must pass through zero; however, the zero lines are situated out of the Fermi surface, because the hole and electron pockets are separated. Moreover, it should be reminded that superconductivity occurs in doped, i.e. disordered systems, so that a scattering on non-magnetic impurities may transfer quasiparticles from the hole to electron sheet and back. Such scattering suppresses superconductivity, similarly to how a scattering on magnetic impurities in conventional superconductors works. However, a different issue is important in this context: a calculated spin–lattice relaxation rate $1/T_1$ in superconductors with $s^{\pm}$ symmetry of the order parameter, in the presence of non-magnetic impurities, changes its exponential temperature dependence into the power-law one, close to $1/T_1 \sim T^{2.5-3}$ [90]. Consequently, an observed power-law temperature dependence of $1/T_1$ might not necessarily imply a non-standard symmetry of the order parameter with gap zeros, but also an existence of coupling with the $s^{\pm}$ symmetry of the order parameter. This concept is supported by the study of superconductivity in FeAs-based systems of other classes, covered by Chaps. 2 and 3, as well as by discussions in the theory-related Chap. 4.

2.4.3 Point-Contact Andreev Reflection

In this method, the current is measured which flows through a point contact of a normal metal to a superconductor, N/S, as function of applied voltage. According to the Blonder–Tinkham–Klapwijk (BTK) theory [118], based on the BCS model with some phenomenological parameters added to account for the quasiparticles damping and the barrier characteristics, the current through the point contact is given by the formula (see [105]):

$$I_{\mathrm{NS}}(V) = C \int [f(E - eV) - f(E)]\,[1 + A(E) + B(E)]\,\mathrm{d}E. \qquad (2.8)$$

Here, $A(E)$ and $B(E)$ are functions determined via modified coherent factors,

$$\widetilde{U}^2 = \frac{1}{2}\left[1 + \frac{\sqrt{(E + i\Gamma)^2 - \Delta^2}}{E + i\Gamma}\right], \quad \widetilde{V}^2 = \frac{1}{2}\left[1 - \frac{\sqrt{(E + i\Gamma)^2 - \Delta^2}}{E + i\Gamma}\right],$$

and C is a constant sensitive to the contact properties on the surface of the superconducting sample. Specifically, it follows:

$$A(E) = |a|^2, \quad B(E) = |b|^2, \quad \text{with}$$
$$a = \widetilde{U}\widetilde{V}/\Gamma\,; \quad b = -(\widetilde{U}^2 - \widetilde{V}^2)(Z^2 + iZ)/\Gamma\,; \quad \Gamma = \widetilde{U}^2 + (\widetilde{U}^2 - \widetilde{V}^2)Z^2\,,$$

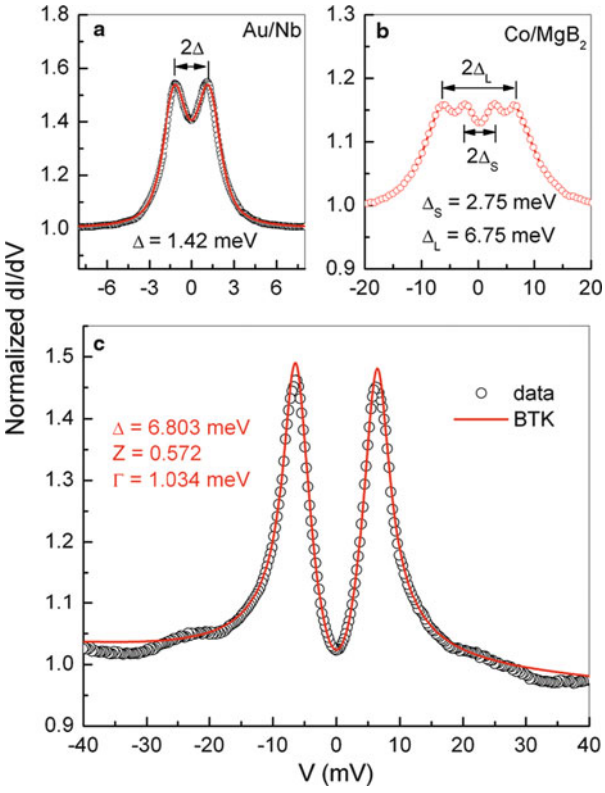

Fig. 2.40 PCAR spectra of superconductors: (**a**) Nb; (**b**) MgB_2; (**c**) $SmO_{0.85}F_{0.15}FeAs$ [105]. In the latter case, the parameters of the BTK model are indicated

which formulae transform into the known Dynes formulae [119] for the tunnel N/S current in the limit of $Z \to \infty$.

As follows from the general formula (2.8), for a conventional superconductor with s symmetry of the gap Δ, the current $I_{NS}(V)$ shows a two-peak structure around $V = 0$, whereby the distance between the spectral peaks equals 2Δ. In Fig. 2.40, an example of a spectrum for the Au/Nb contact is given, where the points mark experimental data and the continuous curve is a result of fitting, with some adjustable parameters added. In Fig. 2.40, the measurement results for the MgB_2 superconductor (the Co/MgB_2 contact) are given.

The observed four maxima reveal the existence of two superconducting gaps, Δ_S (the small one) and Δ_L (the large one). These examples confirm the efficiency of PCAR. Finally, in Fig. 2.40 a spectrum from an $SmO_{0.85}F_{0.15}FeAs$ compound is given, which indicates the presence of just one gap Δ [105]. This spectrum has been obtained for a given point contact on the superconductor surface. In [105], spectra have been collected over 70 point contacts, and their evaluation done by varying the adjustment parameters. The averaged Δ value, obtained with the best

fit, makes $2\Delta = 13.34 \pm 0.3$ meV; hereby, taking into account the value $T_c = 42$ K, we arrive at the estimate $2\Delta/kT_c = 3.68$, quite close to 3.52 value of the BCS theory. Therefore, according to the data of this particular study it appears that the superconductor in question has one isotrop gap, i.e. it is an s-type superconductor. No gap zeros on the Fermi surface seem apparent, and the temperature dependence of $\Delta(T)$ is of conventional BCS type.

In another work [109], more detailed results have been obtained on a sample of $SmO_{0.9}F_{0.1}FeAs$ having $T_c = 51.5$ K. In Fig. 2.41, PCAR spectra are given, recorded in some points at the superconductor surface. In panel c, the results corresponding to two different contacts are shown together from which the presence of two gaps is obvious, $\Delta_1 = 10.5 \pm 0.5$ meV and $\Delta_2 = 3.7 \pm 0.4$ meV. Their temperature dependence is shown in the panel d. Both gaps disappear at the superconducting transition temperature T_c.

A remarkable result is shown in the f panel, where a three-peak structure of spectrum is seen. Beyond two conventional coherent peaks, the so-called zero-bias conductance (ZBC) peak is seen as $V = 0$. It appears due to the formation in the superconducting gap Δ of Andreev bound states, witnessing the existence of zero gap on the Fermi surface. We note that in [105] no such spectra were reported, from which a conclusion was done that the Sm-based superconductors do not have zeros in the superconductor gap.

Since in [109] a ZBP, peak has been detected, a conclusion has been done that the order parameter in the said superconductor has the d symmetry, and all theory curves shown in Fig. 2.41 have been calculated assuming the corresponding angular dependence of the order parameter, $\Delta = \Delta_0 \cos 2\theta$.

As is seen from Table 2.3, also the ZBP peaks were detected in an Nd-containing compound.

A possibility to identify the $s^{\pm}$ gap symmetry in FeAs-type systems with the help of the Andreev reflection was addressed in a row of theory publications [120–124]. In [120], an increase of the density of states at zero energy for an N/$s^{\pm}$ contact was demonstrated; however, this work was mostly numerical one, which made it difficult to establish a relation between the effect announced with a formation of the Andreev bound states in the contact plane. A more complete and physically transparent study was that reported in [123], where the authors generalized the BTK method [118] of phenomenological characterization of contact for the analysis of the Andreev reflection.

The coupled Andreev states appear for both $N/s^{\pm}$ and N/s_{++} contacts, where s_{++} stands for a two-band superconductor in which the signs of the superconducting order parameter coincide on both sheets of the Fermi surface. In Fig. 2.42, the calculated conductance for both cases is shown. The calculation is done for a tunnel contact with $Z = 10$ and the situation with two gaps on the sheets of the Fermi surface, $\Delta_2 = 2\Delta_1$. Moreover, different magnitudes have been considered of the α parameter which gives the ratio of probability amplitudes for an electron coming from a normal metal into superconductor to end up in a state on either electron, or hole surface: $\Psi = \Psi_n + \alpha\psi_e$.

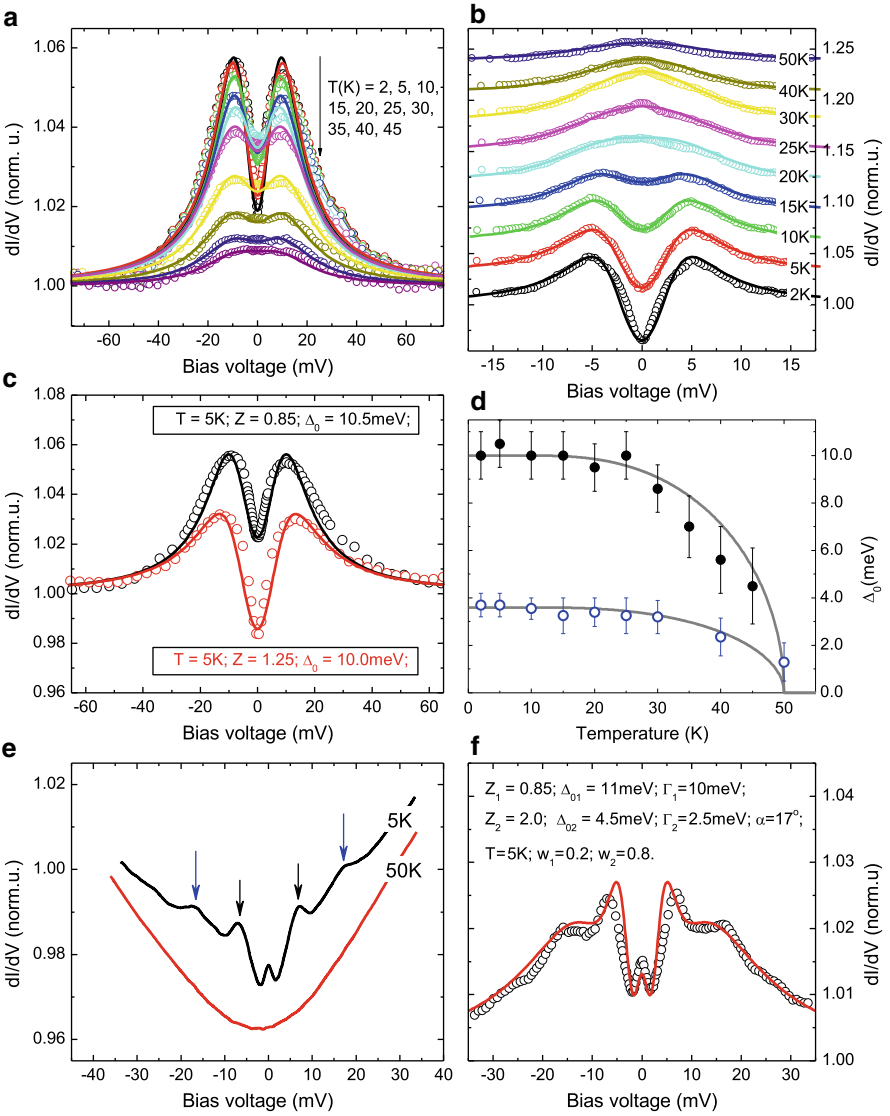

Fig. 2.41 PCAR spectra of superconducting $SmO_{0.9}F_{0.1}FeAs$ [109]. In the (**a**–**c**) and (**f**) panels, the experimental points and theory curves (*solid lines*) with the fitting parameters used are given. (**d**) Temperature dependencies of the gap values determined from fits as shown in (**a**) and (**b**)

As is seen from Fig. 2.42, in the case of $s^{\pm}$ symmetry the peaks in the gap (the smallest one of Δ_1 and Δ_2) due to the formation of bound Andreev states may appear at non-zero values of the potential V. In general, the Andreev bound states may exist in a broad interval of α values: $0 \leq \alpha^2 \leq \Delta_1/\Delta_2$, whereby the ZBP peaks (those at $V = 0$) appear at $\alpha^2 = \Delta_1/\Delta_2$. An emergence of peaks at $V = 0$

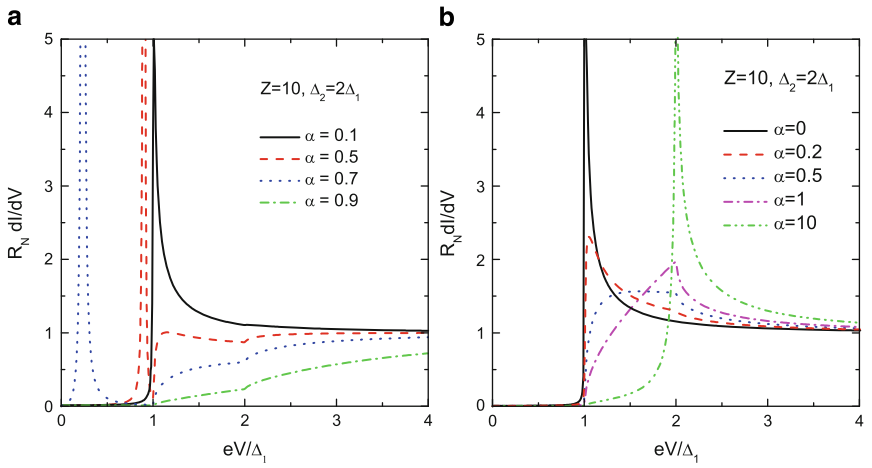

Fig. 2.42 Conductance in the low-transparency regime, (**a**) $N/s^{\pm}$ and (**b**) N/s_{++}, at different values of the α parameter [123]

does not yet mean zeros of the superconducting order parameter, because the $s^{\pm}$ symmetry may be also responsible for the appearance of exactly such peaks. On the other side, an extended s symmetry (the s_{++} one) does not yield bound states in the gap; however, they may exist outside of the latter, and can be erroneously taken for a signature of the multigap state. Summarizing, the observation of ZBP peaks in N/S contacts does not yet unambiguously indicate a presence of zeros in the superconducting order parameter.

Detailed PCAR studies on polycrystalline samples of two superconducting compounds *Re*OFeAs, *Re* = La,Sm, are outlines in [125]. Figure 2.43 shows the measured conductance for two-point contacts, which are characterized by resistivity of the normal metal, R_N, for $LaO_{1-x}F_xFeAs$ at 4.3 K. The experimental data are indicated by dots, whereas continuous curves give the fitting results after the BTK method with a single gap (dashed line) and two gaps (solid line). We see that the observed four-peak structure can be well mapped onto the adjustment curve corresponding to two gaps. Similar results have been obtained for another compound, $SmO_{0.8}F_{0.2}FeAs$, with $T_c = 51.5$ K.

An evaluation of data over numerous contacts results in the following gap values. In $LaO_{1-x}F_xFeAs$, $\Delta_1 \approx 3$ meV, $\Delta_2 \approx 8$–10 meV; in $SmO_{0.8}F_{0.2}FeAs$, $\Delta_1 \approx 6$ meV, $\Delta_2 \approx 19$–20 meV. Hence in both cases, the relation between the large and the small gaps is $\Delta_2/\Delta_1 \approx 3$.

It is remarkable that in no contacts where ZBP peaks detected, so that apparently no gap zeros exist on the Fermi surfaces of these two compounds. On the same contacts from which the data of Fig. 2.43 have been collected, the measurements of conductance have been done at different temperatures (Fig. 2.44), and the temperature dependencies of superconductor gaps $\Delta_1(T)$, $\Delta_2(T)$ extracted. Corresponding curves have also been extracted for the second compound studied, $SmO_{0.8}F_{0.2}FeAs$. Temperature dependencies of the gap for two compounds are markedly different.

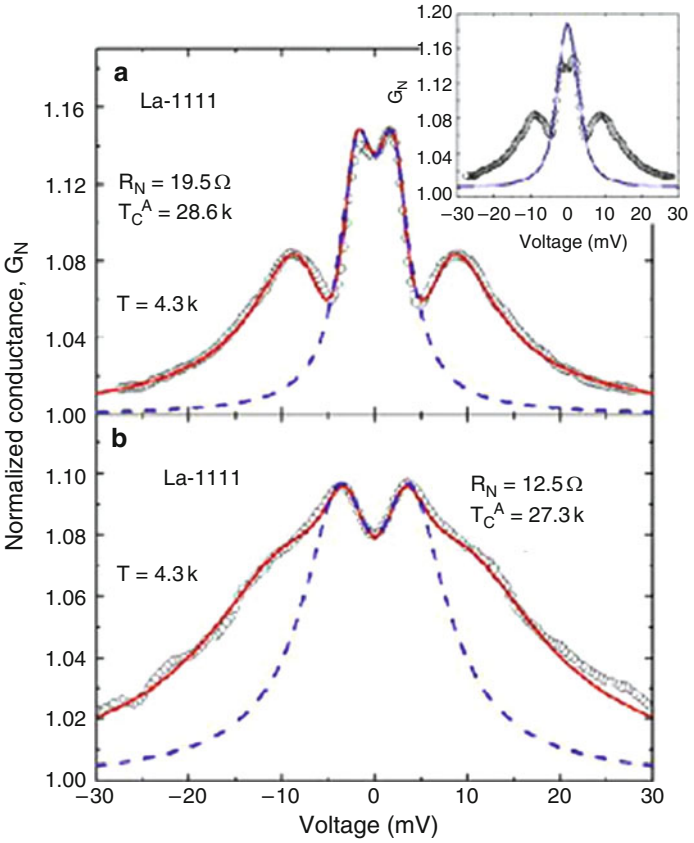

Fig. 2.43 PCAR measurements of conductance for two typical contacts of a $LaO_{1-x}F_xFeAs$ superconductor [125]. In the inset, an adjustment curve corresponding to a suggestion of the *d* symmetry of the superconducting order parameter is given

While in the Sm-containing compound, both gaps close at T_c, the situation in the La-containing compound is more complicated: the larger gap Δ_2 escapes detection already at $T \approx 0.8\,T_c$, whereas the smaller one is still non-zero at $T > T_c$. This situation remains so far obscure; it has been suggested that the Δ_2 may not be necessarily related to a superconducting state. It is interesting to note that in both compounds, the smaller gap is inferior to what could be expected from the BCS theory, namely, $2\Delta_1/kT_c = 2.2$–3.2, whereas the larger gap is substantially beyond the BCS value: $2\Delta_2/kT_c = 6.5$–9.

Even if a number of results obtained is not ultimately clarified, the conclusion remains beyond doubt that the superconductivity occurring in the *Re*OFeAs compounds with *Re* = La and Sm is characterized by the presence of two superconducting gaps, and the absence of gap zeros at the Fermi surface. This superconducting state has an extended *s* symmetry; however, it was not possible to relate the gaps

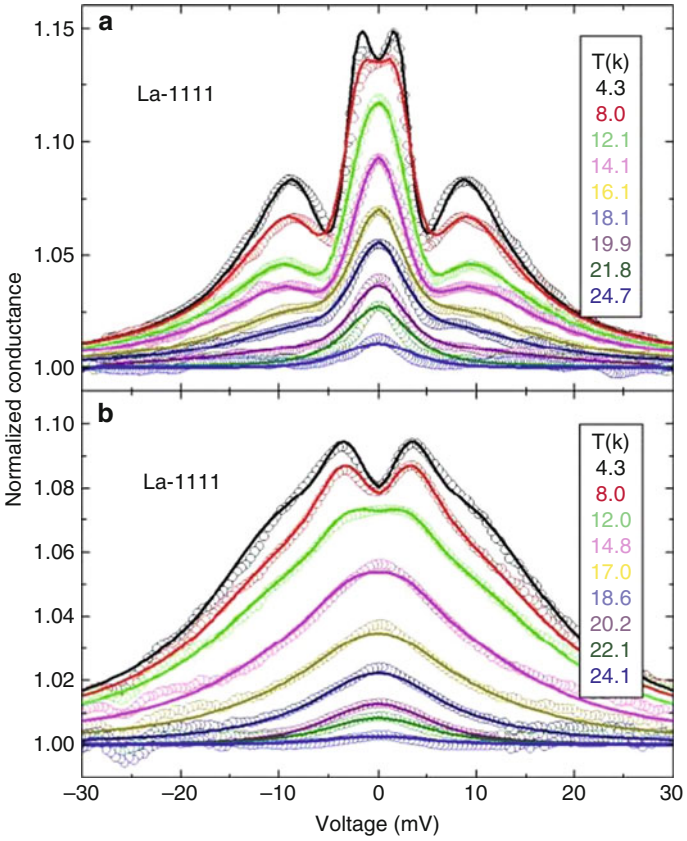

Fig. 2.44 Temperature dependence of conductance for the same point contacts of $LaO_{1-x}F_xFeAs$ which correspond to Fig. 2.43 [125]

Δ_1 and Δ_2 to the hole and electron sheets of the Fermi surface, correspondingly. Moreover, it was not possible to establish a phase relation between the Δ_1 and Δ_2 order parameters. The results so far obtained, however, do not contradict an idea of the $s^{\pm}$ symmetry of the superconducting order parameter in the *Re*OFeAs compounds. Very pronounced ZBP was discovered in $TbO_{09}F_{0.1}FeAs$ [127].

In another work [126], done on the $LaO_{1-x}Fe_xFeAs$ compound using the PCAR method, three energy gaps have been detected: two superconducting gaps $\Delta_1 = 2.8$–4.6 meV and $\Delta_2 = 9.8$–12 meV, which do not possess zeros at the Fermi surface, and a pseudogap which survives at temperatures by far exceeding T_c, up to $T^* \sim 140$ K, that is close to the Néel temperature for the undoped compound. This pseudogap is, probably, induced by spin fluctuations, which exist in doped superconducting compounds above T_c.

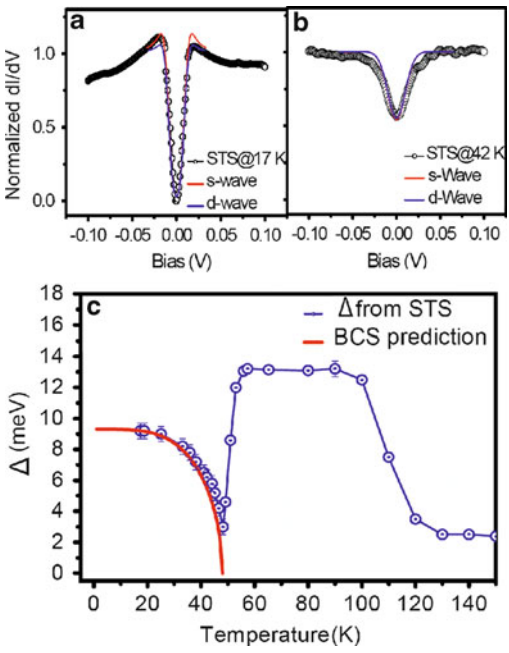

Fig. 2.45 STS-study of $NdO_{0.86}F_{0.14}FeAs$ [110]. (**a**) Tunnel spectrum at $T = 17\,\mathrm{K}$; (**b**) tunnel spectrum at $T = 42\,\mathrm{K}$; (**c**) temperature dependence of the superconducting gap Δ and the pseudogap Δ_{PG}s

2.4.4 Tunnel and Photoemission Spectroscopies (STS, PES, ARPES)

As an example, we discuss the results obtained for the $NdO_{0.86}F_{0.14}FeAs$ compound with $T_c = 48\,\mathrm{K}$ [110] by the scanning tunnel spectroscopy method. The tunnel spectra obtained at 17 K show a suppression of the electron density within $\pm 10\,\mathrm{meV}$, whereby two gaps of the widths 9 and 18 meV are revealed. They both close at T_c, but only one of them follows in its behaviour the Dynes formula [119] for the tunnel current. Remarkably, at $T > T_c$ another gap, of not superconducting nature, is detected; it emerges drastically at $T = T_c$ and remains unchanged throughout a broad temperature range up to 120 K (Fig. 2.45).

The temperature dependence of the pseudogap is completely different from that in cuprates, where the pseudogap appears due to the interaction of electrons with spin fluctuations. The same interaction is responsible for the Cooper pairing; hence, the superconducting gap and the pseudogap are driven by the same mechanism and do overlap as the temperature varies. In the sample studied of the above FeAs-type compound, the pseudogap disappears as the superconductor gap opens, so that they seem to be quasi in competition. The nature of this phenomenon is not so far clarified, although it may be suggested that the pseudogap is also related to spin fluctuations.

In another STS study, that of the $SmO_{0.85}FeAs$ compound with $T_c = 52\,\mathrm{K}$ [108], the V-shaped gaps in the spectrum were well mapped on the theory curves

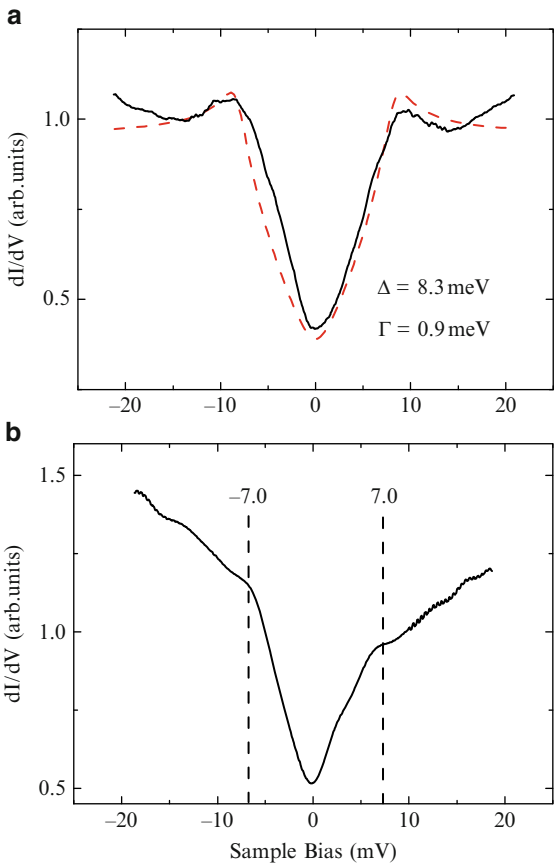

Fig. 2.46 Tunneling spectra of the $SmO_{0.85}FeAs$ at 4.2 K taken (**a**) in a region where coherence peaks were observed and (**b**) in a region where only sharp gap edges were found with a peak at $V = 0$, revealing a presence of zeros in the superconducting gap [108]

corresponding to the d symmetry of the order parameter. In some cases, ZBP peaks at $V = 0$ have been detected, which are compatible with the d symmetry of the order parameter (Fig. 2.46).

The superconducting compound $NdO_{0.86}F_{0.14}FeAs$, hence with the composition very close to that discussed above and $T_c = 53$ K, was studied by ARPES [111]. The only gap of about 13–18 meV has been detected on the hole sheet of the Fermi surface around the Γ point. The measurements at different angles to the crystallographic axes of the FeAs plane revealed a certain anisotropy (Fig. 2.47).

An inspection of Table 2.3 brings us to a conclusion that the data concerning the symmetry of the superconductor order parameter are, as of now, not conclusive. The most studied so far is the $LaO_{1-x}F_xFeAs$ system. All NMR measurements give a power-law dependence $1/T_1 \sim T^3$ which cannot be unambiguously interpreted: it may signify either the presence of gap zeros on the Fermi surface, or, in the presence of nonmagnetic impurities, the $s^{\pm}$ type of symmetry. PCAR investigations of this system give contradictory results as well. Aiura et al. [115] argues towards the s type

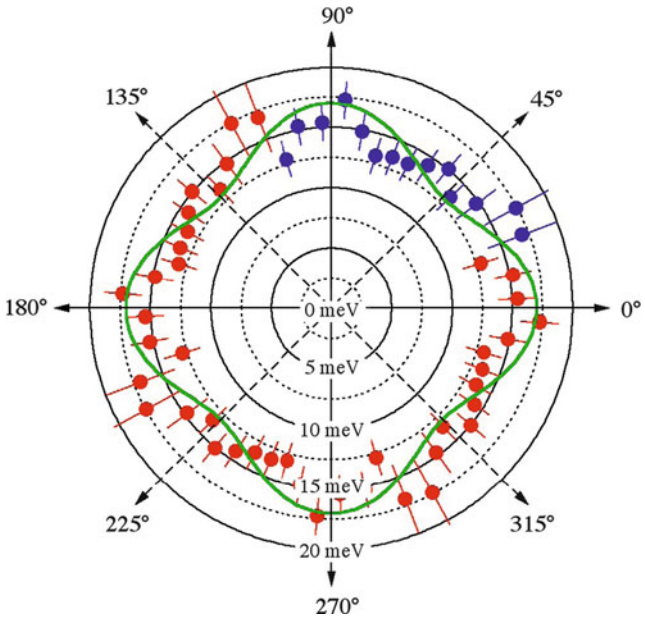

Fig. 2.47 Superconducting gap on a hole sheet of the Fermi level, centred at Γ, after the ARPES study of a $NdO_{0.9}F_{0.1}FeAs$ single crystal at $T = 20$ K [111]

symmetry, whereas [128] reports ZBC peaks, corresponding to the presence of gap zeros. In Nd-, Sm- and Pr-containing systems, the situation is equally ambiguous.

At the same time, none of the results gained by different methods seem to contradict the suggestion about the $s^{\pm}$ symmetry of the order parameter. An ultimate conclusion could have been done following the analysis of the data obtained for other FeAs-type systems, considered in the Chaps. 2 and 3. We note a single important fact following from Table 2.3: in many cases, the pseudogap is detected at temperatures substantially superior to the T_c. Previously, such phenomenon has been detected in cuprates, and now it rests to verify whether its nature in FeAs-related systems is the same, i.e. whether it is due to interactions of electrons (or holes) with spin fluctuations.

http://www.springer.com/978-3-642-14529-2

High-Tc Superconductors Based on FeAs Compounds

Izyumov, Y.; Kurmaev, E.

2010, XI, 278 p., Hardcover
ISBN: 978-3-642-14529-2